THE ASTROPHYSICAL JOURNAL, 445:642–659, 1995 June 1

OXYGEN ABUNDANCES IN DIFFUSE ELLIPTICALS AND THE METALLICITY-LUMINOSITY RELATIONS FOR DWARF GALAXIES

MICHAEL G. RICHER[1,2] AND MARSHALL L. MCCALL[1,2]
Centre for Research in Earth and Space Science, York University, 4700 Keele Street, North York, Ontario, Canada M3J 1P3
Received 1994 August 25; accepted 1994 December 7

ABSTRACT

We have obtained spectroscopy of planetary nebulae in the dwarf irregular galaxy NGC 6822 and the diffuse elliptical galaxies NGC 185 and NGC 205. We have also introduced a new dwarf irregular metallicity-luminosity relation based upon a more homogeneous treatment of distances and abundances. Supplementing our best estimates of the mean oxygen abundance for NGC 185 and NGC 205 with existing data for the planetary nebula in Fornax, we find that the oxygen abundances in diffuse ellipticals exceed those in comparably luminous dwarf irregulars by at least 1.5 times the dispersion in our new metallicity-luminosity relation. When we combine our oxygen abundances with iron abundances from the literature, we find that NGC 185, NGC 205, and Fornax have [O/Fe] ratios that are roughly solar or higher, on average. These [O/Fe] ratios are larger than those in dwarf irregulars if the [O/Fe] ratios observed in the Magellanic Clouds are typical of those in other dwarf irregulars, which indicates that the star formation timescale in diffuse ellipticals is much shorter than that in dwarf irregulars. Therefore, while oxygen abundances allow diffuse ellipticals to be the evolved remnants of dwarf irregulars, [O/Fe] ratios indicate that an evolutionary connection is unlikely because they have fundamentally different star formation histories.

Subject headings: galaxies: abundances — galaxies: elliptical and lenticular, cD — galaxies: irregular — planetary nebulae: general

1. INTRODUCTION

From photometric studies of their core properties, diffuse elliptical galaxies (i.e., galaxies with elliptical-like stellar populations, but with exponential surface brightness profiles, such as NGC 205 or dwarf spheroidal galaxies) appear to be more closely related to dwarf irregular galaxies than to normal $r^{1/4}$-law ellipticals (Kormendy 1985; Binggeli & Cameron 1992). Consequently, it has been proposed that diffuse ellipticals formed through the removal of the gas in dwarf irregulars either through ram-pressure stripping, supernova-driven galactic winds, or star formation (see Kormendy & Djorgovski 1989 and references therein). The anticorrelation of the dwarf irregular and diffuse elliptical spatial distributions observed in the Virgo Cluster (Binggeli, Tammann, & Sandage 1987) argues that an environmental effect is operating to transform dwarf irregulars into diffuse ellipticals. Dekel & Silk (1986) have suggested that both diffuse ellipticals and dwarf irregulars have had much of their original gas expelled by supernova blast waves but that dwarf irregulars managed to retain some fraction of their gas. On the other hand, Bothun et al. (1986) argue that the surface brightness of dwarf irregulars is already too low to allow them to fade to become diffuse ellipticals. Clearly, an important test of the genealogy of diffuse ellipticals, and this paper's primary objective, is a comparison of the metallicities in diffuse ellipticals and dwarf irregulars (Wirth & Gallagher 1984).

Consider the following possible scenario. A dwarf irregular destined to become a diffuse elliptical forms successive generations of stars until its gas supply is either exhausted through star formation or removed by other means, and then it fades as its stellar population ages (e.g., Renzini & Buzzoni 1986). In this scenario, diffuse ellipticals are the "mature" form of dwarf irregulars. Diffuse ellipticals formed in this way should follow a metallicity-luminosity relation similar to that observed for dwarf irregulars (e.g., Kinman & Davidson 1981; Skillman, Kennicutt, & Hodge 1989a) but which is shifted to lower luminosity. Consequently, at a fixed luminosity, diffuse ellipticals should appear more metal-enriched than dwarf irregulars because diffuse ellipticals would have evolved from more luminous dwarf irregulars.

Consider a diffuse elliptical and a dwarf irregular that have the same luminosity today. If the diffuse elliptical has a higher metallicity than the dwarf irregular, it is possible, but not necessary, that it was once a dwarf irregular. If the diffuse elliptical has a lower metallicity, however, it could never have been a dwarf irregular similar to those that define the metallicity-luminosity relation. Thus, a comparison of the metallicities in diffuse ellipticals and dwarf irregulars can be used to assess whether it is possible for diffuse ellipticals to have evolved from dwarf irregulars.

There have been several attempts to address the issue of the metallicities in diffuse ellipticals and dwarf irregulars (e.g., Skillman et al. 1989a), and it has been concluded that diffuse ellipticals and dwarf irregulars follow the same metallicity-luminosity relation (i.e., same slope and zero point). This claimed coincidence of the metallicity-luminosity relations, however, is strongly dependent on the value of [O/Fe] adopted for diffuse ellipticals. In diffuse ellipticals, it is the stellar iron abundance that is known, but in dwarf irregulars, it is the H II region oxygen abundance that is known. Using these data to compare the metallicities of diffuse ellipticals and dwarf irregulars presents a severe problem: an O/Fe ratio must be adopted to convert the diffuse elliptical iron abundances to oxygen abundances. Oxygen is the more reliable chemical evolution indicator because Type II supernovae are its principal source (Wheeler, Sneden, & Truran 1989). [O/Fe] varies over

[1] Observations reported in this paper were obtained at the Multiple Mirror Telescope Observatory, a joint facility of the University of Arizona and the Smithsonian Institution.

[2] Visiting Astronomer, Canada-France-Hawaii Telescope, operated by the National Research Council of Canada, le Centre National de la Recherche Scientifique de France, and the University of Hawaii.

time within a given galaxy and depends sensitively on its star formation history (Gilmore & Wyse 1991). For stars in the [Fe/H] regime occupied by diffuse ellipticals, [O/Fe] $\sim +0.45$ in the Milky Way (Tomkin et al. 1992), but [O/Fe] ~ -0.3 in the Magellanic Clouds (Russell & Dopita 1992). This metallicity range allows the diffuse elliptical metallicity-luminosity relation to be shifted up to 6 mag fainter than the dwarf irregular metallicity-luminosity relation (see § 4.1).

To circumvent the [O Fe] problem, we propose to use planetary nebulae as probes of the stellar oxygen abundance in both dwarf irregulars and diffuse ellipticals. Bright planetary nebulae are particularly useful as chemical evolution probes since they are found in all types of galaxies. Most notably, they are presently the only direct oxygen abundance probes available in galaxies without active star formation.

Recently, Richer (1993) showed that bright planetary nebulae (in [O III] λ5007) in the Magellanic Clouds are good oxygen abundance probes. This conclusion is based upon two observations. First H II regions and bright planetary nebulae in the Magellanic Clouds have identical mean oxygen abundances. Second, for oxygen abundances up to at least solar, the [O III] λ5007 fluxes from planetary nebulae increase as the oxygen abundance increases. Consequently, the oxygen abundances for the brightest planetary nebulae are biased toward the highest oxygen abundances present in the population (Richer 1993; Dopita, Jacoby, & Vassiliadis 1992). Given these properties, bright planetary nebulae must, like H II regions, sample a recent star formation event from a chemical evolution viewpoint and should be good probes of the latest state of chemical evolution in galaxies.

Since planetary nebulae are the death phase of intermediate-mass stars, however, one might worry that the prior evolution of their progenitors may have modified their original oxygen abundances. The similarity of the mean oxygen abundances in Magellanic Cloud planetary nebulae and H II regions rules out the possibility that planetary nebula precursors consume much of their initial oxygen (Richer 1993). If the precursors consumed any significant fraction of their initial envelope oxygen abundance to produce nitrogen, their initial abundances must have exceeded those observed in H II regions today. Also, it is unlikely that precursors produce significant amounts of oxygen since planetary nebulae follow a neon-oxygen relation that is almost identical to that followed by extragalactic H II regions (Henry 1989; Vigroux, Stasinska, & Comte 1987). Since Type II supernovae dominate the production of both oxygen and neon (Wheeler et al. 1989), the abundances of these elements should be strongly correlated if neither is subsequently modified. Theoretically, only the most massive intermediate-mass stars, which undergo the second dredge-up (Iben & Renzini 1983), are expected to produce planetary nebulae whose oxygen abundances could differ significantly from their initial oxygen abundance (type I; see Peimbert & Torres-Peimbert 1983). While observations do not rule out the conversion of oxygen to nitrogen in the progenitors of type I planetary nebulae, they do indicate that this conversion is not the dominant mode of nitrogen production, since even type I planetary nebulae appear to follow the normal neon-oxygen relation (Henry 1989).

In this paper, we will use planetary nebulae to determine oxygen abundances in the nearby diffuse ellipticals NGC 205 and NGC 185 and compare these abundances with those in comparably luminous dwarf irregulars. In § 2, we present our spectroscopic data for planetary nebulae in the diffuse ellipticals NGC 185 and NGC 205 and the dwarf irregular NGC 6822. We use this data in § 3 to derive the oxygen abundance in NGC 6822. In § 3 we also develop empirical methods that allow us to set lower limits on the oxygen abundance in NGC 185 and NGC 205. These lower limits are based upon empirical relations between the nebular oxygen abundance and the maximum [O III] λ5007 luminosity and [O III] λ5007/Hβ ratio attained. In § 4, we introduce a new metallicity-luminosity relation for dwarf irregulars and use our estimates of the oxygen abundance in NGC 185, NGC 205, and Fornax to constrain the relationship between diffuse ellipticals and dwarf irregulars. We also use our oxygen abundance estimates to constrain the [O/Fe] ratio in diffuse ellipticals and consider its implications regarding their formation. Finally, we summarize our conclusions in § 5.

2. OBSERVATIONS AND ANALYSIS

2.1. *Observations and Reductions*

Our spectroscopic data were obtained at the Multiple Mirror Telescope (MMT) and the Canda-France-Hawaii Telescope (CFHT). At the MMT, we observed NGC 185 and NGC 205. At the CFHT, we observed NGC 205 and NGC 6822. On both occasions, clouds and poor seeing hampered observations, so we only present relative fluxes. Table 1 presents a log of all of the observations.

Our MMT data were obtained on 1991 October 30 (UT). The red spectrograph was used with a 150 lines mm^{-1} grating, whose blaze wavelength is 4800 Å in first order. Coupled with a 1″ slit, this setup yielded a resolution of 20 Å. The detector was an 800 × 800 Texas Instruments CCD with 15 μm pixels. The total spectral coverage was 4250–7440 Å. The spectra were flux-calibrated using observations of BD +28°4211 and IC 418. Dome flat fields and arc lamp spectra were acquired at the beginning and end of the night. The spectrograph slit was oriented so that it included the two brightest planetary nebulae in each galaxy.

Our CFHT data were obtained on 1992 August 22–23 using the MOS/SIS imaging spectrograph in multiobject (MOS) mode. MOS/SIS is a multiobject, imaging, grism spectrograph (see Le Fèvre et al. 1994 for a description) that uses focal plane masks constructed from previously acquired images. The masks are created on-line using a YAG laser. The object slits were chosen to be 1″ wide by 14″ long. We used a 600 lines mm^{-1} grism (B600) that gave a dispersion of 105 Å mm^{-1} and a central wavelength of 4950 Å. The detector was the STIS (Tektronix) 1024 × 1024 CCD, which has 21 μm pixels. The spatial scale at the detector was 0.″43 pixel^{-1}. The spectral coverage varied for each object, depending on the object's location within the field of view. The wavelength coverage was effectively truncated blueward of $\sim$4300 Å because of the CCD response and redward of $\sim$6740 Å because of object posi-

TABLE 1

OBSERVATION LOG

Date	Observatory	Object	Exposure Time (s)	N^a
1991 October 30.....	MMT	NGC 185	1800	3
		NGC 205	2700	2
1992 August 23	CFHT	NGC 6822	1200	3
		NGC 6822	1800	2
		NGC 205	1200	2

[a] Number of exposures.

TABLE 2

LINE INTENSITIES

IDENTIFICATION	NGC 185, PN 1 (MMT)				NGC 185, PN 2 (MMT)				NGC 205, PN 5 (MMT)				NGC 205, PN 6 (MMT)				NGC 205, PN 4 (CFHT)			
	F	δF	I	δI	F	δF	I	δI	F	δF	I	δI	F	δF	I	δI	F	δF	I	δI
Hβ	100	11	100	11	100[a]	...	100	...	100[a]	...	100	...	100[a]	...	100	...	100	36	100	36
[O III] λ4959	265	23	255	22	348	100	342	99	530	132	528	132	408	90	405	89	487	129	486	129
[O III] λ5007	770	61	730	58	1103	226	1076	220	1394	331	1388	330	1251	225	1237	223	1593	407	1585	407
Hα	454	38	280	23	350	91	280	73	291	68	280	66	310	53	280	48	...	...	...	...
$E(B-V)$	0.422	...	...	...	0.195[b]	...	...	...	0.035[b]	...	...	...	0.088[c]	...	...	...	0.035[b]	...	...	...

IDENTIFICATION	NGC 205, PN 2 (CFHT)				NGC 205, PN 3 (CFHT)				NGC 205, PN 7 (CFHT)				NGC 205, PN 8 (CFHT)				NGC 205, PN 9 (CFHT)			
	F	δF	I	δI	F	δF	I	δI	F	δF	I	δI	F	δF	I	δI	F	δF	I	δI
Hγ	53	13	54	13	...	...	...	...	...	...	...	...	...	...	...	...	...	...	...	...
[O III] λ4363	18	11	18	11	...	...	...	...	...	...	...	...	...	...	...	...	...	...	...	...
Hβ	100	10	100	10	100	17	100	17	100	12	100	12	100	24	100	24	100	7	100	7
[O III] λ4959	367	27	366	27	161	21	160	21	320	28	319	28	447	78	446	78	278	16	277	16
[O III] λ5007	1188	84	1182	84	518	62	516	62	974	85	970	85	1572	268	1565	268	877	47	873	47
He I λ5876	17	5	16	5	...	...	...	...	23	4	22	4	...	...	...	...	16	4	16	4
$E(B-V)$	0.035[b]	...	...	...	0.035[b]	...	...	...	0.035[b]	...	...	...	0.035[b]	...	...	...	0.035[b]	...	...	...

IDENTIFICATION	NGC 205, PN 5 (CFHT)				NGC 205, PN 6 (CFHT)				NGC 205, PN 10 (CFHT)				NGC 6822, S16 (CFHT)				NGC 6822, S33 (CFHT)			
	F	δF	I	δI	F	δF	I	δI	F	δF	I	δI	F	δF	I	δI	F	δF	I	δI
Hδ	...	...	...	...	...	...	...	...	...	...	...	...	...	...	...	...	20	5	26	6
Hγ	36	12	37	12	...	...	...	...	...	...	...	...	28	6	33	7	33	3	39	3
[O III] λ4363	26	11	27	11	...	...	...	...	...	...	...	...	18	5	21	6	21	2	24	3
He II λ4686	...	...	...	...	...	...	...	...	...	...	...	...	23	5	24	5	53	2	55	2
Hβ	100	15	100	15	100	13	100	13	100	9	100	9	100	14	100	14	100	2	100	2
[O III] λ4959	418	44	417	44	401	36	398	36	437	29	426	29	386	37	372	36	374	5	361	5
[O III] λ5007	1275	134	1269	134	1278	114	1263	114	1378	88	1329	88	1229	119	1165	113	1144	17	1084	16
He I λ5876	16	4	16	4	22	6	21	6	6	3	5	3	22	3	15	2	...	...	...	...
[N II] λ6548	...	...	...	...	8	16	8	16	19	4	14	4	...	...	...	...	...	...	...	...
Hα	266[d]	112	256	112	310	34	280	34	388	25	280	25	...	...	...	...	...	...	...	...
[N II] λ6583	...	...	...	...	69	17	63	17	53	5	38	5	...	...	...	...	...	...	...	...
$E(B-V)$	0.035[b]	...	...	...	0.088	...	...	...	0.285	...	...	...	0.42[e]	...	...	...	0.42[e]	...	...	...

[a] Estimated from the Hα intensity and the reddening.
[b] Reddening from Burstein & Heiles 1984.
[c] Reddening from the CFHT spectrum.
[d] Hα intensity based upon [O III] λ5007/Hα from the MMT spectrum.
[e] Reddening from van den Bergh & Humphreys 1979.

tioning. Typically, the Hγ–He I λ5876 spectral range was observed at a dispersion of 2.2 Å pixel^{-1}. Spectra were calibrated using observations of Hiltner 102 and Feige 110. Arc lamp spectra and flat-field exposures of the spectrograph's internal map were interspersed among the observations of each object.

The spectra were reduced using the routines in IRAF[3] following the procedures described in the IRAF documents by Anderson (1987) ("noao.twodspec" package, for NGC 205 at the MMT) and Massey, Valdes, & Barnes (1992) ("noao.imred.specred" package, for the other data). First, all of the images were corrected for overscan bias, zero-level (bias pattern), and pixel-to-pixel response variations. At this point, the MMT images of NGC 205 were aligned and co-added before extracting one-dimensional spectra. These spectra were then flux-calibrated using the standard star observations. For the other data, individual object spectra were first extracted and calibrated. Then, the spectra from each image were combined to produce the final spectra for each object.

2.2. *Line Intensities*

Table 2 presents the line intensities for all of the planetary nebulae observed. The object names and finder charts may be found in Ford, Jenner, & Epps (1973) for NGC 185 and NGC 205 and Killen & Dufour (1982) for NGC 6822. We confirm that the stellar object S16 in the Killen & Dufour (1982) catalogue of diffuse nebulae and emission-line stars is a planetary nebula. This object is unresolved in direct CFHT images, having a full width at half maximum $\sim 1''.3$, and it shows strong He II λ4686 emission in its spectrum. Thus, S16 doubles the number of known planetary nebulae in NGC 6822.

For each object, Table 2 lists the observed line ratios, F, the reddening-corrected line ratios, I, and their errors δF and δI, respectively. The Schild (1977) reddening law ($R = 3.2$) was used to correct for reddening. In all cases, we assumed an intrinsic Hα/Hβ ratio of 2.8 (Osterbrock 1989), which is valid for electron temperatures and densities of approximately 15,000 K and 4000 cm^{-3}, respectively, conditions typical for bright planetary nebulae in the Magellanic Clouds (e.g., Meatheringham & Dopita 1991a, b). We did not use the Hγ/Hβ ratio to derive reddenings (see below). The observed and reddening corrected line intensities are related by

$$\log \frac{F(\lambda)}{F(\mathrm{H}\beta)} = \log \frac{I(\lambda)}{I(\mathrm{H}\beta)} - 0.4E(B-V)[A(\lambda) - A(\mathrm{H}\beta)] , \quad (1)$$

where $A(\lambda)$ is the reddening at wavelength λ from Schild (1977). If the Hα/Hβ ratio could not be measured from the spectrum, we adopted reddening values from Burstein & Heiles (1984) for NGC 185 and NGC 205, but from van den Bergh & Humphreys (1979) for NGC 6822.

The line intensities were measured using a locally implemented software package (McCall 1982). The line intensities were measured relative to Hβ for the CFHT data, but relative to Hα for the MMT data. The only reliable Hβ detection among our MMT data is that for PN 1 in NGC 185, but it is weak. For the MMT data, we calculated line ratios relative to Hβ after adopting the reddenings listed in Table 2 and assuming Hα/Hβ = 2.8.

Comparing our CFHT data for S33 in NGC 6822 with those of Dufour & Talent (1980), it appears that our flux calibration is incorrect between Hδ and Hβ. For S33, we observe systematically lower line intensities between Hδ and Hβ than do Dufour & Talent (1980). The reddenings implied by our Hγ/Hβ ratios for S33 and S16 are unreasonably large compared to other reddening estimates for NGC 6822. We have been unable to determine the source of this calibration problem, but it is not underlying Balmer absorption from stars in NGC 6822. The planetary nebulae were observed through short slits, so the sky subtraction would have accounted for any underlying stellar absorption. Furthermore, Balmer absorption would cause Hδ/Hβ to be even more discrepant than Hγ/Hβ, which it is not. Fortunately, the [O III] lines are adjacent to hydrogen lines, so their relative intensities are unaffected by this calibration problem because the intrinsic ratios of the hydrogen lines are known. However, this flux calibration problem prevents us from using Hγ/Hβ ratios to determine foreground reddenings.

Apart from the Hδ to Hβ wavelength region, we believe that our flux calibration is free of problems. As a check on our flux calibration at the MMT, we obtained a spectrum of IC 418. Our observed Hα/Hβ ratio for IC 418 was 3.67, very similar to other measurements in the literature (e.g., Kohoutek & Martin 1981; Torres-Peimbert & Peimbert 1977). PN 6 in NGC 205 is the only object we observed at both telescopes, and the [O III] λ5007/Hα line ratios from both data sets are the same within errors. Thus, we conclude that the CFHT flux calibration is correct between Hβ and Hα, and we believe that our Hα-based reddening estimates are trustworthy.

Comparing our MMT and CFHT data, it is obvious that the latter enjoy higher signal-to-noise ratios. As a result, we adopted the CFHT line ratios for PN 5 and PN 6 in NGC 205.

Our reddening for PN 1 in NGC 185 is larger than the foreground reddening estimated by Burstein & Heiles (1984), but is otherwise not unusual given that planetary nebulae suffer from internal reddening. PN 10 in NGC 205 may also suffer a similar amount of internal reddening, but PN 5 and PN 6 in NGC 205 apparently suffer very little internal reddening since their reddenings are comparable to the Burstein & Heiles (1984) foreground value. The two planetary nebulae in NGC 6822 also appear to suffer little reddening owing to either internal dust or dust within NGC 6822.

3. OXYGEN ABUNDANCES

3.1. *The Planetary Nebulae in NGC 6822*

We detected the temperature-sensitive [O III] λ4363 line in both planetary nebulae in NGC 6822. For our electron temperature calculations, we adopted an electron density of 4000 cm^{-3}, which is typical for bright planetary nebulae in the Magellanic Clouds (Meatheringham & Dopita 1991a, b). From the line intensities in Table 2, we find an [O III] temperature of 17,100 ± 2800 K in S16 and 17,600 ± 1200 K in S33. Using Dufour & Talent's (1980) data for S33, we find an [O III] temperature of 19,200 ± 1600 K for our adopted electron density. Although these temperatures only barely agree, the exact cause of their difference is not obvious. All temperatures were computed using the code FIVEL (De Robertis, Dufour, & Hunt 1987).

Our abundance calculations follow the ionization correction factor (ICF) approach of Torres-Peimbert & Peimbert (1977) and are described in Richer (1993). For S33, we adopted Dufour & Talent's (1980) [O II] λ3727, He II λ4686, and He I λ5876 line intensities. From these data, we find 12 + log (O/

[3] IRAF is distributed by the National Optical Astronomy Observatories, which is operated by the Associated Universities for Research in Astronomy, Inc., under contract to the National Science Foundation.

H) = 8.10 ± 0.08 for S33. For S16, we obtain 12 + log (O^{2+}/H) = 8.01 ± 0.16 (we did not observe any lines of O^+). The main source of error in these abundances is the uncertainty in the [O III] λ4363 line strength, which dominates the error in the temperature. Changing the density by an order of magnitude in these abundance calculations changes the derived oxygen abundances by 0.02 and 0.04 dex in S16 and S33, respectively.

These planetary nebula abundances are similar to those observed in H II regions in NGC 6822. In H II regions with measured temperatures, the mean oxygen abundance is 12 + log (O/H) = 8.23 (see Table 5). Thus, as in the Magellanic Clouds, H II regions and bright planetary nebulae have similar mean oxygen abundances.

3.2. *The Planetary Nebulae PN 2 and PN 5 in NGC 205*

Our best [O III] λ4363 detection was for PN 2 in NGC 205. Even for this object, we can only determine a lower limit to the oxygen abundance since we did not observe any lines of O^+. We find that the electron temperature is 13,300 ± 3300 K, so 12 + log (O^{2+}/H) = 8.21 ± 0.20. For PN 5, our [O III] λ4363 line intensity is best regarded as an upper limit. Thus, we find an upper limit of 15,300 K for the electron temperature and a lower limit for the abundance of 12 + log (O^{2+}/H) ≥ 8.11. For both of these objects, the ICF should be small since we did not detect He II λ4686. The corollary, however, is that the O^+ contribution is likely to be significant. As usual, we adopted an electron density of 4000 cm^{-3} for all of these calculations.

3.3. *Empirical Abundance Techniques*

3.3.1. *Justification*

For both planetary nebulae in NGC 185 and all of those in NGC 205, save PN 2, we did not detect [O III] λ4363, so we cannot derive their electron temperatures or oxygen abundances directly. Consequently, we shall derive lower limits to the abundances in these objects through empirical techniques based upon the properties of planetary nebulae in the Milky Way and the Magellanic Clouds. To obtain our lower limits, we make use of the observations that, for these planetary nebulae, the maximum [O III] λ5007 luminosities and the maximum [O III] λ5007/Hβ ratios attained are functions of the nebular oxygen abundance. The details of these two techniques will be developed in the following two sections, but here we would like to demonstrate that it is reasonable to obtain oxygen abundance limits using the calibration of these techniques based upon planetary nebulae in the Milky Way and the Magellanic Clouds (the data samples will be defined in the following section).

As a planetary nebula evolves, both its [O III] λ5007 luminosity and its [O III] λ5007/Hβ ratio will change as a result of its central star's evolution. Consequently, it is important to investigate whether the temperatures and luminosities of the planetary nebula central stars in NGC 185 and NGC 205 are similar to those in the Milky Way and the Magellanic Clouds. This issue is particularly worrisome because the planetary nebulae in NGC 185 and NGC 205 undoubtedly arise from an older stellar population than those from which the planetary nebulae in the Magellanic Clouds and the Milky Way arise. To help address this issue, Figure 1 presents the reddening-corrected [O III] λ5007/Hβ ratios plotted as a function of the total Hβ luminosities for all Milky Way and extragalactic planetary nebulae for which these data exist. The region to the right of the diagonal line in Figure 1 includes all objects whose [O III] λ5007 luminosities are within 2 mag of the brightest planetary nebula in the LMC. In Figure 1, the Hβ luminosities for the planetary nebulae in NGC 185 and NGC 205 were

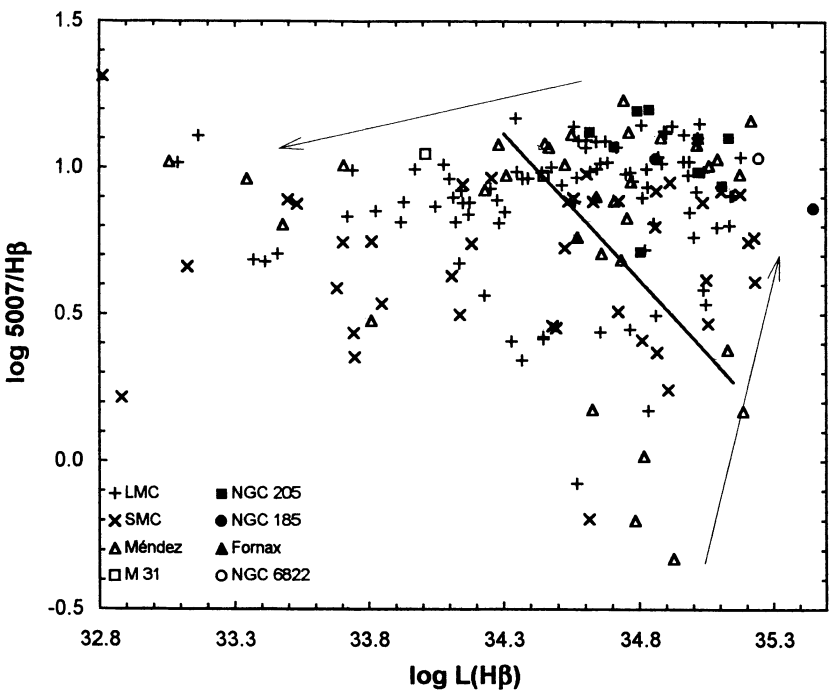

FIG. 1.—A comparison of the global properties of planetary nebulae in diffuse ellipticals with those in star-forming systems. Planetary nebulae in different galaxies are represented by different symbols, as indicated in the legend. The diagonal line separates bright and faint objects: those to the right of the line all have [O III] λ5007 luminosities within 2 mag of that for the brightest planetary nebula in the LMC. The two arrows denote the two evolutionary tracks discussed in the text.

calculated using our spectral data and the [O III] λ5007 fluxes from Ciardullo et al. (1989), adopting the distance moduli given in Table 5, and foreground reddenings of 0.19 mag and 0.035 mag for NGC 185 and NGC 205, respectively (Burstein & Heiles 1984).

Figure 1 is similar to an H-R diagram for planetary nebula central stars. Insofar as planetary nebulae are optically thick to ionizing radiation (see Mendez, Kudritzki, & Herrero 1992 for a discussion), the Hβ luminosity is a measure of the central star's ionizing luminosity. The [O III] λ5007/Hβ ratio, meanwhile, is sensitive to the central star temperature for temperatures below $\sim 10^5$ K, although it is also sensitive to the nebular oxygen abundance (see § 3.3.3). In Figure 1, the central star evolution should cause the Hβ luminosities and [O III] λ5007/Hβ ratios to vary in the manner shown by the arrows. Despite significant scatter, the region occupied by planetary nebulae in Figure 1 is similar to that expected.

In Figure 1, the planetary nebulae in NGC 185 and NGC 205 are not conspicuously anomalous in any way, so their properties are not grossly different from those of bright planetary nebulae in the Galaxy and the Magellanic Clouds. As a result, it is not unreasonable to constrain the abundances of planetary nebulae in NGC 185 and NGC 205 using limits derived from the maximum [O III] λ5007 luminosities and [O III] λ5007/Hβ ratios observed in Milky Way and Magellanic Cloud planetary nebulae.

3.3.2. *Oxygen Abundances from* [O III] λ5007 *Fluxes*

The first method we will use to obtain lower limits to the oxygen abundances for planetary nebulae in NGC 185 and NGC 205 is based upon the work of Richer (1993), who found that the maximum [O III] λ5007 luminosity observed in Magellanic Cloud planetary nebulae varied as a function of the nebular oxygen abundance. To demonstrate the generality of this relation, the [O III] λ5007 luminosities of the planetary nebulae shown in Figure 1 are plotted as a function of their oxygen abundance in Figure 2. The symbols have the same meaning as in Figue 1.

Our empirical abundance techniques are calibrated using the following samples of planetary nebulae in the Magellanic Clouds and the Milky Way. The Magellanic Cloud planetary nebula data comprises the compilation from Richer (1993) supplemented by the data from Vassiliadis et al. (1992) and Jacoby & Kaler (1993). We computed abundances for the Vassiliadis et al. (1992) objects using the ionization correction factor scheme described earlier. The Galactic planetary nebulae are a subset of those studied by Méndez et al. (1992) (those for which oxygen abundances exist). For these, we adopted the extinction-corrected Hβ luminosities and [O III] λ5007/Hβ ratios given by Méndez et al. (1993). Further, to help gauge the generality of our calibrations, we have included data for planetary nebulae in M31, NGC 6822, and the Fornax diffuse elliptical. The spectral data for planetary nebulae in M31 were taken from Jacoby & Ford (1986), while their luminosities were derived from the [O III] λ5007 fluxes in Ford & Jacoby (1978) and Ciardullo et al. (1989). For S33 in NGC 6822, we adopted the oxygen abundance obtained above and the Hβ flux from Dufour & Talent (1980). The data for the planetary nebula in Fornax were taken from Maran et al. (1984). To calculate absolute luminosities, we adopted the distance moduli listed in either Table 5 or the Appendix, the Schild (1977) reddening law, corrected to a ratio of total-to-selective extinction of $R = 3.07$, and foreground Galactic reddenings, $E(B-V)$, of 0.019 mag, 0.035 mag, 0.093 mag, 0.033 mag, and 0.42 mag for

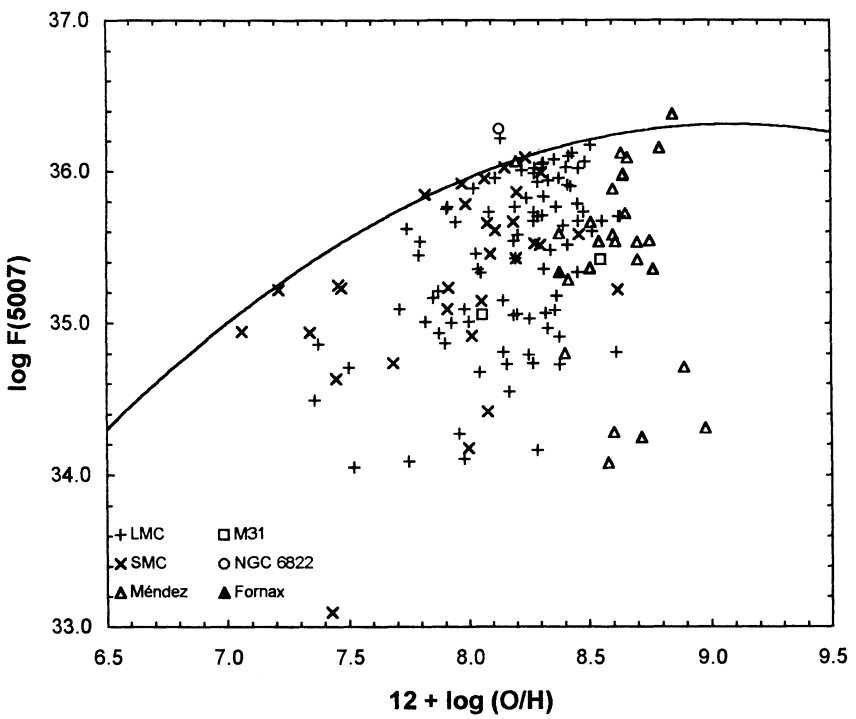

FIG. 2.—This figure shows the basis of our [O III] λ5007 luminosity-based oxygen abundances. The line is a relation that Dopita et al. (1992) derived from a series of nebular models. Here, we have shifted their relation so that it fits the maximum [O III] λ5007 flux observed as a function of oxygen abundance for Magellanic Cloud planetary nebulae. Our luminosity-based oxygen abundance limits are computed by assuming that a planetary nebula has the lowest oxygen abundance allowed for its [O III] λ5007 flux.

the SMC, the LMC, M31, Fornax, and NGC 6822, respectively (McNamara & Feltz 1980; McClure & Racine 1969; van den Bergh 1969; Burstein & Heiles 1984; Buonanno et al. 1985; van den Bergh & Humphreys 1979).

Richer (1993) noted that the maximum [O III] λ5007 luminosity varied with abundance according to a relation that Dopita et al. (1992) derived from a set of nebular models. Shifting their relation to agree with the maximum [O III] λ5007 luminosities observed for Magellanic Cloud planetary nebulae, the maximum attainable [O III] λ5007 luminosity, log $L(5007)_{max}$, depends upon oxygen abundance according to

$$\log L(5007)_{max} = 11.46 + 5.47x - 0.301x^2 + 0.4(\mu_{LMC} - 18.372) , \quad (2)$$

where $x = 12 + \log (O/H)$ and μ_{LMC} is the distance modulus of the LMC (here, we use $\mu_{LMC} = 18.372$; see the Appendix). Thus, a measurement of the [O III] λ5007 luminosity yields a lower limit to the oxygen abundance. Equation (2) is shown as a solid line in Figure 2. Henceforth, we shall refer to the oxygen abundance limits given by equation (2) as *luminosity limits*.

Three objects significantly exceed the limit defined by equation (2) and are found above the line in Figure 2: SMP 62 in the LMC, S33 in NGC 6822, and NGC 7027. *Hubble Space Telescope* observations show that LMC SMP 62 has a very bright central star (Blades et al. 1992), which may explain its position in Figure 2. As noted earlier, the [O III] λ5007 luminosity for S33 in NGC 6822 is based upon a spectroscopic Hβ flux (§ 3.3.1), so it could easily be significantly in error (see Jacoby & Kaler 1993 for a good discussion). Finally, Masson (1989) quotes an uncertainty of 17% on the distance for NGC 7027, which can easily account for its position. Thus, equation (2) appears to give a reliable limit to the maximum [O III] λ5007 luminosity achievable in the oxygen abundance range spanned by the objects in Figure 2.

Although equation (2) is based upon the expected efficiency with which planetary nebulae emit [O III] λ5007 (Dopita et al. 1992) and despite the good match between equation (2) and the upper envelope in Figure 2, one might worry that the upper envelope in Figure 2 is due to a systematic variation in age rather than oxygen abundance. Because the oxygen abundance in the interstellar medium increases with time, the most oxygen-rich planetary nebulae arise from the youngest progenitors. Thus, the progenitors of oxygen-rich planetary nebulae are more massive than the progenitors of planetary nebulae with lower abundances. If the properties of planetary nebula central stars are sensitive to the progenitor mass, the upper envelope in Figure 2 could be the result of systematic differences in progenitor mass rather than the result of a change in abundance. Fortunately, in addition to the discussion in the previous section, two other pieces of evidence indicate that [O III] λ5007 luminosities are not sensitive to the age of the progenitor population.

The similarity of the [O III] λ5007 luminosities of planetary nebulae in the SMC and LMC in the abundance range where they overlap, $8.0 \leq 12 + \log (O/H) \leq 8.3$, is the first indication that [O III] λ5007 luminosities do not depend upon the age of their progenitors. The SMC planetary nebulae in this abundance range have abundances near the interstellar medium oxygen abundance, so they are undoubtedly products of recent star formation. The LMC planetary nebulae with these abundances, particularly those with abundances near $12 + \log (O/H) \sim 8.0$, have abundances considerably lower than the interstellar medium value (Richer 1993), so they must come from an older star formation event. Thus, the LMC planetary nebulae with abundances near $12 + \log (O/H) \sim 8.0$ must have less massive progenitors than the SMC planetary nebulae with this abundance. Despite this, these LMC and SMC planetary nebulae have similar maximum [O III] λ5007 luminosities. Consequently, the age of the planetary nebula progenitors does not seem to affect the maximum [O III] λ5007 luminosity.

The luminosities of planetary nebulae in M31's bulge also argue that the age of the stellar population producing the planetary nebulae does not affect [O III] λ5007 luminosities. In M31, the (absolute) peak luminosity of the planetary nebulae luminosity function (PNLF) is $M^*_{5007} = -4.44$ mag while, in the LMC, it is $M^*_{5007} = -4.15$ mag [adopting $\mu_0 = 24.286$ mag, $E(B-V) = 0.093$ mag, and $m^*_{5007} = 20.17$ mag for M31, $\mu_0 = 18.372$ mag, $E(B-V) = 0.035$ mag, and $m^*_{5007} = 14.35$ mag for the LMC, and the Schild 1977 reddening law adjusted to $R = 3.07$: see Appendix; Ciardullo et al. 1989; Jacoby, Walker, & Ciardullo 1990]. Thus, despite the older stellar population in the bulge of M31, its PNLF reaches higher luminosities than does that of the LMC. Undoubtedly, the oxygen abundances in the bulge of M31 are higher than those in the LMC. Equation (2) would predict a peak luminosity difference of the magnitude observed between the LMC and M31 if M31's bulge planetary nebulae have a mean oxygen abundance of $12 + \log (O/H) \sim 8.8$ dex, a reasonable estimate given preliminary spectral data (Kaler 1994).

Therefore, the available evidence indicates that our luminosity limits should be applicable to the planetary nebulae in NGC 185 and NGC 205 even though these objects arise from a stellar population that is undoubtedly older than that from which the planetary nebulae in the Milky Way and Magellanic Clouds arise.

3.3.3. *Oxygen Abundances from* [O III] λ5007/Hβ *Ratios*

It is also possible to obtain a lower limit to the oxygen abundance using the observed [O III] λ5007/Hβ ratio. Figure 3 shows the basis of this method. In this figure, the reddening-corrected [O III] λ5007/Hβ ratio is plotted as a function of oxygen abundance for extragalactic and Milky Way planetary nebulae. In addition to the objects in Méndez et al. (1993), our Milky Way planetary nebula sample includes the data from Torres-Peimbert & Peimbert (1977), Aller & Keyes (1987), Kingsburgh (1992), the halo objects from Henry (1989), and the objects from Webster (1988) for which [O III] temperatures could be obtained. This collection of Milky Way data is in no way comprehensive, but it does sample a wide variety of objects with relatively little overlap. The data for all of these objects were adopted directly from the literature without modification or reanalysis. When there were several measurements of the oxygen abundance and [O III] λ5007/Hβ ratio for one object, the most recent was usually chosen. As was the case for the [O III] λ5007 luminosities (Fig. 2), the [O III] λ5007/Hβ ratio has a well-defined upper limit at a given oxygen abundance.

To define the upper envelope drawn by the solid curve in Figure 3, the data were first divided into abundance bins 0.1 dex wide. Next, we computed the mean [O III] λ5007/Hβ ratio for all points within 0.3 dex of the largest value in each bin. We then fit a quadratic to the mean [O III] λ5007/Hβ ratio in each bin, using only values within 0.3 dex of the maximum value to compute the means. This 0.3 dex cutoff was chosen by examining a histogram of the [O III] λ5007/Hβ ratios with respect to

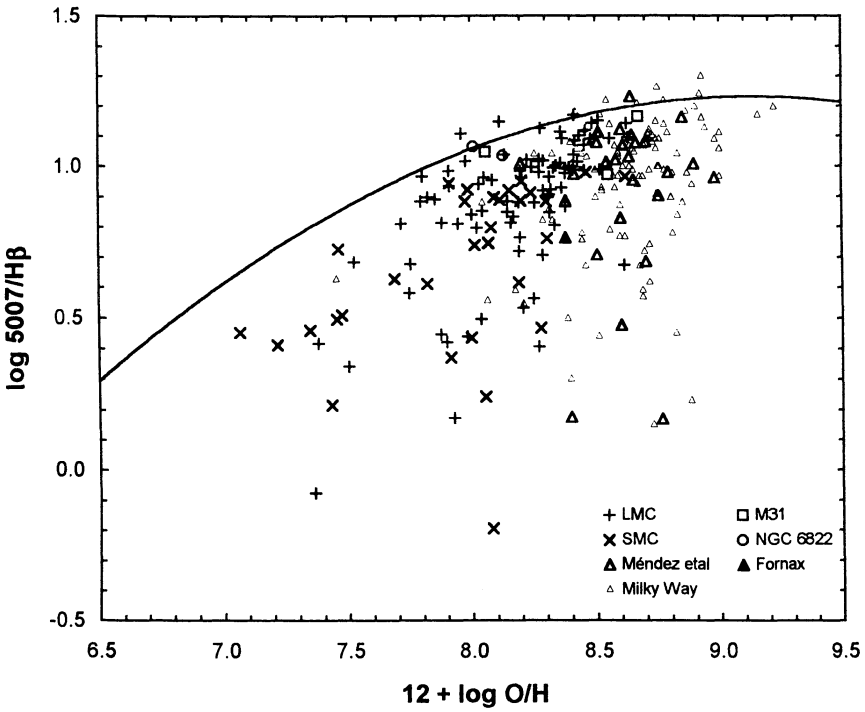

FIG. 3.—This figure demonstrates the principle underlying our [O III] λ5007/Hβ-based oxygen abundances. The derivation of the line drawn as an upper limit is described in the text. Again, we arrive at our [O III] λ5007/Hβ-based abundance limits by assuming that a planetary nebula has the lowest oxygen abundance permitted for its observed [O III] λ5007/Hβ ratio.

the largest value in each bin. A histogram of these relative [O III] λ5007/Hβ ratios shows a very peaked distribution with 73% of the points within 0.3 dex of the maximum value, but with a long tail to lower [O III] λ5007/Hβ ratios. The mean of the relative [O III] λ5007/Hβ ratios within the first 0.3 dex was −0.145. To obtain the relation betwen the maximum observed [O III] λ5007/Hβ ratio and abundance, we shifted the quadratic fit to the mean [O III] λ5007/Hβ ratios upward by 0.145 dex. The resulting relation is given by

$$\log [\text{O III}]\ \lambda 5007/\text{H}\beta = (-10.05 \pm 7.26) + (2.47 \pm 1.73)x + (-0.135 \pm 0.103)x^2 , \quad (3)$$

where $x = 12 + \log (\text{O/H})$. The fit was performed over the range $7.7 \leq 12 + \log (\text{O/H}) < 9.1$, the range over which there were at least three objects per abundance bin. To check for galaxy-to-galaxy variations, we computed the mean relative [O III] λ5007/Hβ ratio within the top 0.3 dex separately for the Milky Way, the LMC, and the SMC. The resulting values were −0.15, −0.13, and −0.16, respectively. Results of Student's *t*-tests show that the SMC mean is significantly different from the mean for the LMC, so we excluded the SMC data set in the derivation of equation (3). Henceforth, we shall refer to the oxygen abundance limits given by equation (3) as *ratio limits*.

As Figure 3 shows, very few points exceed the upper limit given by equation (3). Over the abundance range we used to define our upper limit, $7.7 \leq 12 + \log (\text{O/H}) < 9.1$, only 12 out of 175 planetary nebulae exceed this limit. If we model the distribution of points exceeding the bin means with the normal distribution, our upper limit corresponds approximately to a 1.5 σ limit.

Since the [O III] λ5007/Hβ ratio is independent of distance, it is simpler to use as an abundance indicator than the [O III] λ5007 luminosity. Eliminating the distance constraint is beneficial because it allows us to use Milky Way planetary nebulae to define the behavior of the [O III] λ5007/Hβ ratio at high oxygen abundances. In addition, the [O III] λ5007/Hβ ratio is almost independent of reddening, e.g., a reddening of 1 mag increases the [O III] λ5007/Hβ ratio by only 0.06 dex (Schild 1977 reddening law). Another benefit of the [O III] λ5007/Hβ ratio is that it is relatively unaffected by whether the nebula is optically thick or thin. Limited tests, using the nebular modeling code CLOUDY (Ferland 1991), indicate that log [O III] λ5007/Hβ is not significantly affected by bounding until the nebula is truncated in the inner half of the O^{2+} zone. Thus, equation (3) is even applicable for nebulae that are very optically thin.

A minor drawback of the ratio limits compared to the luminosity limits is that equation (3) has a shallower slope. Thus, small errors in [O III] λ5007/Hβ will have a greater effect on the abundance limits derived from equation (3) than similar errors would have upon limits based upon equation (2). However, errors in [O III] λ5007/Hβ are much smaller than errors in [O III] λ5007 luminosities, particularly when systematic errors associated with distance moduli and reddening are considered.

3.3.4. *Limit Choice and How to Use It*

Generally, the luminosity and ratio limits on the oxygen abundance for any given planetary nebula will be different. This is not surprising, considering how planetary nebula central stars evolve. The luminosity limit to the oxygen abundance (eq. [2]) will be closest to the actual abundance for a planetary nebula that is at its peak [O III] λ5007 luminosity. Likewise, the ratio limit (eq. [3]) is closest to the actual abundance for planetary nebulae with [O III] λ5007/Hβ ratios at the

TABLE 3

OXYGEN ABUNDANCE LIMITS

Method	LMC	SMC	Milky Way	NGC 205	NGC 185	Fornax
Number of planetary nebulae	49	16	12	9	2 or 3	1
Mean luminosity limit	7.82	7.74	7.96	8.02	7.83	7.28
Mean ratio limit	7.82	7.41	8.03	8.06	7.70	7.27
Mean maximum of limits	7.97	7.78	8.17	8.23	...	7.28
Observed planetary nebula mean	8.28	8.15	8.60	$\geq$8.21	...	8.38
Observed – maximum	0.31	0.38	0.42	...	...	...
Estimated planetary nebula mean	8.34	8.15	8.54	8.60	8.20	7.98

maximum allowed. Figure 1 shows that these maxima do not occur simultaneously.

The simplest approach to obtain a lower limit to the mean oxygen abundance in a galaxy is to take the mean of the individual lower limits for all of the planetary nebulae. The mean of the lower limits will be a lower limit to the mean, provided that the individual lower limits are all lower than the actual abundances. To test this technique, we applied it to the Magellanic Cloud and the Milky Way data sets. Within each data set, we considered all planetary nebulae within 2 mag of the brightest, since this is approximately the luminosity range spanned by the planetary nebulae in NGC 205. This is also, roughly, the completeness limit of the three data sets (Jacoby et al. 1990; Méndez et al. 1993). For these objects, we computed lower limits to the oxygen abundance based upon their [O III] λ5007 luminosities and [O III] λ5007/Hβ ratios. Using these data, we selected the larger of the two limits for each planetary nebula, the *maximum limits*, and used these to compute a lower limit to the mean oxygen abundance for each galaxy. Table 3 lists the mean maximum limit along with separate means for the luminosity and ratio limits. In addition, the actual mean abundance for the luminosity range is given. In all three cases, selecting the larger of the individual lower limits for each object and taking the mean of these gives the lower limit closest to the actual mean abundance. On average, however, even this best estimate is still 0.37 dex below the actual abundance (Table 3).

The difference between the actual abundance and the lower limit is largest for our Milky Way sample, which is the most metal-rich. At high abundances, the slopes of equations (2) and (3) are shallower. Thus, it clearly helps to have large planetary nebula samples at high oxygen abundances.

3.4. *Empirical Oxygen Abundances in NGC 185 and NGC 205*

Table 4 lists our abundance limits for each planetary nebula we observed in NGC 185 and NGC 205. The fifth column in Table 4 lists the luminosity limits, while the sixth column lists the ratio limits. For reference, Table 4 also lists the [O III] λ5007 luminosity and the [O III] λ5007/Hβ ratios for each planetary nebula. The [O III] λ5007 luminosities listed for the planetary nebulae in NGC 185 and NGC 205 in Table 4 are from Ciardullo et al. (1989).

Following our experience with the Milky Way and Magellanic Cloud data sets, we computed the mean maximum limit for the nine planetary nebulae in NGC 205. The lower limit to the mean oxygen abundance in NGC 205 derived from this technique is $12+\log(\mathrm{O/H}) \geq 8.23$, which is listed in Table 3 (Mean Maximum of Limits). Table 3 also lists the lower limits to mean oxygen abundance for the planetary nebulae in NGC 205 derived from the luminosity and ratio limits. Note that these lower limits for NGC 205 are in excellent agreement with the lower limit for PN 2 based upon the measurement of [O III] λ4363, which is listed as the "Observed PN Mean" in Table 3.

Although these empirical techniques can be applied to the nine planetary nebulae in NGC 205 with confidence, PN 1 in NGC 185 presents an obstacle to their application to the two planetary nebulae in NGC 185. The [O III] λ5007 luminosity of PN 1 in NGC 185 exceeds the maximum luminosity predicted by equation (2), so it is impossible to derive a luminosity limit for this object. Consequently, PN 1 was excluded in computing the luminosity limit given in Table 3. However, to increase the sample size, the other two planetary nebulae in NGC 185 with [O III] λ5007 luminosities within 2 mag of that of PN 1 were included in the calculation of the luminosity limit. Thus, the ratio limit includes both PN 1 and PN 2, but the luminosity limit includes PN 2, PN 3, and PN 5, even though there is no spectroscopy for the latter two. The mean of the luminosity limits, $12+\log(\mathrm{O/H}) \geq 7.83$, is larger than the mean of the ratio limits for NGC 185, so the luminosity limit will be adopted as the lower limit to the mean abundance for the planetary nebulae in NGC 185.

We believe that our lower limits of $12+\log(\mathrm{O/H}) \geq 7.83$ and $12+\log(\mathrm{O/H}) \geq 8.23$ for NGC 185 and NGC 205, respectively, are excessively conservative. In the Milky Way and the Magellanic Clouds, the actual mean oxygen abundances are, on average, 0.37 dex higher than the largest of the lower limits. We can think of no reason why a similar difference should not exist for NGC 185 and NGC 205, particularly since the mean oxygen abundances implied by our lower limits are similar to

TABLE 4

DATA FOR EXTRAGALACTIC PLANETARY NEBULAE

GALAXY	PN	I(5007) [I(Hβ) = 1]	log L(5007)[a] (ergs s^{-1})	12+log (O/H)[b] L(5007)	12+log (O/H)[b] 5007/Hβ
Fornax[c]		5.80	35.33	7.28	7.27
NGC 185.....	1	7.30	36.32	9.09	7.48
	2	10.76	35.89	7.91	7.92
	3	...	35.78	7.76	...
	5	...	35.84	7.83	...
NGC 205.....	2	11.82	35.78	7.76	8.05
	3	5.16	35.52	7.46	7.17
	4	15.85	36.04	8.13	8.65
	5	12.69	36.24	8.58	8.16
	6	12.63	36.12	8.29	8.15
	7	9.69	36.00	8.07	7.79
	8	15.65	35.99	8.05	8.61
	9	8.73	36.05	8.15	7.67
	10	13.29	35.74	7.71	8.24

[a] Calculated from the galaxy distances in Table 5, the reddenings given in the text, the [O III] λ5007 fluxes of Ciardullo et al. 1989 for NGC 185 and NGC 205, and the Hβ flux and [O III] λ5007/Hβ ratio from Maran et al. 1984 for Fornax.

[b] Empirical lower limits to the oxygen abundance based upon equations (2) and (3).

[c] All data from Maran et al. 1984.

those in the Milky Way and Magellanic Cloud data sets. Thus, we believe that increasing our lower limits by 0.37 dex, to $12+\log(O/H) = 8.20$ and $12+\log(O/H) = 8.60$ in NGC 185 and NGC 205, respectively, provides the most reasonable estimates of the mean oxygen abundances in their planetary nebulae. The case for a high mean oxygen abundance in NGC 205 is particularly compelling, since its abundance limits in Table 3 are all slightly larger than those for the Milky Way sample, whose actual abundance is $12+\log(O/H) = 8.60$. Furthermore, a high abundance for NGC 205 would lend support to the work of Davidge (1992), who found that the metallicity of asymptotic giant branch (AGB) stars in NGC 205 appeared to be near solar.

3.5. *Fornax*

The Fornax diffuse elliptical is the only other diffuse elliptical for which there is spectral information for its planetary nebula "population." The most complete chemical abundance analysis of its planetary nebula is that of Maran et al. (1984), who obtained $12+\log(O/H) = 8.38$. However, we would like to guard against the possibility that the oxygen abundance in this planetary nebula may be atypically high compared to the stellar population. To do this, we note that, for planetary nebulae within 2 mag of the brightest, the abundance dispersion is $\sigma = 0.20$ dex in the LMC, $\sigma = 0.16$ dex in the SMC (Richer 1993), and $\sigma = 0.16$ dex for our Milky Way sample. Also, of the planetary nebulae within 2 mag of the brightest in the Milky Way, the LMC, and the SMC, SMP 19 in the SMC exceeds the mean oxygen abundance by the largest amount, 1.9 σ. Therefore, if we allow that the planetary nebula in Fornax is a 2 σ point and set $\sigma = 0.20$ dex, we obtain an estimate of the mean abundance in Fornax of $12+\log(O/H) \geq 7.98$. We adopt this limit as our best estimate of the mean oxygen abundance for stars in the Fornax diffuse elliptical. Table 3 lists this limit as our "Estimated PN Mean." Table 3 also lists the other empirical limits. To compute the luminosity and ratio limits, we adopted Maran et al.'s (1984) Hβ flux and [O III] λ5007/Hβ ratio.

4. DISCUSSION

4.1. *Comparison with Dwarf Irregulars*

The most straightforward way to determine whether diffuse ellipticals can evolve from dwarf irregulars is to determine whether they follow the same metallicity-luminosity relation. Since this comparison is so important, we have determined a new dwarf irregular metallicity-luminosity relation using only the best available data for dwarf irregulars. To qualify, a dwarf irregular must have had a well-determined distance and an oxygen abundance based upon a measured [O III] temperature. These data for the qualifying galaxies are listed in

TABLE 5

ABUNDANCES AND LUMINOSITIES OF DWARF IRREGULARS AND DIFFUSE ELLIPTICALS

Galaxy	$12+\log(O/H)$	Sources	DM[a]	Sources	M_B	Distance Method[b]
Fornax	7.98	Table 3	20.61	22	−11.69	HB
GR 8	7.63	7, 16	25.16	23	−10.52	Blue stars
Holmberg II	7.92	9	27.65	24	−16.13	Cepheids in NGC 3031
IC 10	8.22	6	25.40	25	−16.79	Blue stars
IC 1613	7.71	18	24.27	26	−14.42	Cepheids
IC 2574	8.08	9, 18	27.65	24	−16.85	Cepheids in NGC 3031
IC 4662	8.09	3	27.11	27	−15.64	Red stars
Leo A	7.36	14	25.77	28	−12.93	Blue stars
LMC	8.35	15	18.37	29	−17.73	SN 1987A
NGC 1560	8.02	8	26.87	30	−16.17	Blue stars
NGC 1569	8.16	18	26.19	25	−16.34	Blue stars
NGC 185	8.20	Table 3	23.98	31	−14.61	HB
NGC 205	8.60	Table 3	24.68	32	−15.89	HB
NGC 2366	7.92	5, 9, 12, 18	27.26	26	−15.79	Cepheids in NGC 2403
NGC 3109	8.06	8	25.25	33	−14.82	TRGB
NGC 4214	8.23	9, 18, 19	28.03	34	−17.82	Blue stars
NGC 5408	8.01	13, 20	27.55	35, 36	−15.60	Mean of SBF and PNLF for NGC 5128
NGC 55	8.34	13, 18, 21	25.73	37	−18.07	Carbon stars
NGC 6822	8.23	6, 10, 11, 17, 18	23.39	26, 38, 39	−14.88	Mean of TRGB and Cepheids
Sextans A	7.55	14	25.33	26	−13.53	Cepheids
Sextans B	8.12	7	25.38	26	−13.73	Cepheids
SMC	8.03	15	18.85	40	−16.35	Cepheids
UGC 6456	7.86	19	27.65	24	−13.24	Cepheids in NGC 3031
WLM	7.80	17	24.67	26, 41	−13.73	Mean of TRGB and Cepheids

NOTES.—Abundance sources: (1) French 1980; (2) Gonzalez-Riestra, Rego, & Zamorano 1988; (3) Heydari-Meyalari, Melnick, & Martin 1990; (4) Kinman & Davidson 1981; (5) Kennicutt, Balick, & Heckman 1980; (6) Lequeux et al. 1979; (7) Moles, Aparicio, & Masegosa 1990; (8) M. McCall & M. Richer, unpublished results; (9) Masegosa, Moles, & del Olmo 1991; (10) Peimbert & Spinrad 1970; (11) Pagel, Edmunds, & Smith 1980; (12) Peimbert, Pena, & Torres-Peimbert 1986; (13) Stasinska, Comte, & Vigroux 1986; (14) Skillman et al. 1989a; (15) Russell & Dopita 1992; (16) Skillman et al. 1988; (17) Skillman, Terlevich, & Melnick 1989b; (18) Talent 1980; (19) Tully et al. 1981; (20) Terlevich et al. 1991; (21) Webster & Smith 1983.

Distance modulus sources: (22) Buonanno et al. 1985; (23) Aparico, Garcia-Pelaya, & Moles 1988; (24) NGC 3031, see Appendix; (25) Karachentsev & Tikhonov 1994; (26) Madore & Freedman 1991; (27) Heydari-Malayeri et al. 1990; (28) Sandage 1986; (29) see Appendix; (30) Lee & Madore 1993; (31) Saha & Hoessel 1990; (32) Saha, Hoessel, & Krist 1992; (33) Lee 1993; (34) Sandage & Tammann 1982; (35) Hui et al. 1993; (36) Tonry & Schechter 1990; (37) Pritchet et al. 1987; (38) McAlary & Welch 1985; (39) Lee, Freedman, & Madore 1993a; (40) Freedman 1988; (41) Lee, Freedman, & Madore 1993b.

[a] Distance modulus.

[b] Distance method codes are as follows: "blue stars" denotes the brightest three blue stars; "HB" denotes the horizontal branch stars; "PNLF" denotes the planetary nebula luminosity function; "red stars" denotes the brightest three red stars; "SBF" denotes surface brightness fluctuations; "TRGB" denotes the tip of the red giant branch.

Table 5 along with our adopted absolute B magnitudes, the sources for the distance moduli and abundances, and the method by which each galaxy's distance was established. Our adopted distances are all based upon stellar properties. Our rationale and calibration of these distances are discussed in the Appendix, and we refer the reader there for these details. Absolute B magnitudes are founded upon the apparent B magnitudes given in de Vaucouleurs et al. (1991). Abundances for the dwarf irregulars were computed following the prescription given in § 3.1. For ease of comparison, Table 5 also lists the same data for Fornax, NGC 185, and NGC 205.

Our dwarf irregular metallicity-luminosity relation is shown in Figure 4. The principal difference between our metallicity-luminosity relation and that of Skillman et al. (1989a) is that we find more scatter at low luminosities, though we find less at high luminosities. The onset of this scatter seems to occur abruptly at $M_B \sim -15$ and seems to be one-sided: the scatter in low-luminosity galaxies, $M_B > -15$, is toward high abundances. This characteristic implies that the scatter is not a result of poor [O III] λ4363 detections since this would more likely bias the electron temperatures to high values and lead to lower abundances. A least-squares fit to the more luminous galaxies, $M_B < -15$, yields a relation that is similar to that of Skillman et al. (1989a),

$$12+\log (\mathrm{O/H}) = (5.67 \pm 0.48) + (-0.147 \pm 0.029) M_B , \quad (4)$$

but which is shifted to slightly lower luminosities so that we find somewhat higher abundances at the same luminosity. The dispersion about this metallicity-luminosity relation is 0.08 mag for $M_B < -15$. Equation (4) is plotted as a solid line in Figure 4.

In Figure 4 we have also plotted NGC 185, NGC 205, and Fornax using our adopted mean oxygen abundances. Clearly, the oxygen abundances in these diffuse ellipticals are systematically higher than those of similarly luminous dwarf irregulars. On average, their oxygen abundances exceed the abundances predicted by equation (4) by 0.5 dex. Even using our conservative lower limits from Table 3, the oxygen abundances in NGC 185, NGC 205, and Fornax would exceed those in comparably luminous dwarf irregulars by 0.13 dex, 1.5 times the dispersion in equation (4). Given how extremely conservative these lower limits are, we find it inescapable that diffuse ellipticals have higher abundances than similarly luminous dwarf irregulars.

The fundamental result of Figure 4 is that our adopted abundances, by themselves, *allow* that diffuse ellipticals may evolve from dwarf irregulars. If one adopts the view that diffuse ellipticals evolve from irregulars, one can calculate the amount by which diffuse ellipticals have faded. Based upon our adopted abundances for NGC 185, NGC 205, and Fornax, these galaxies have faded by at least 3 to 4 mag, on average. Note, however, that if the stars in Fornax have an oxygen abundance similar to that measured for its planetary nebula, Fornax has faded by more than 6 mag. Four magnitudes of fading can occur within 1 Gyr and 6 mag within a few Gyr (e.g., Bruzual & Charlot 1993). These timescales are reasonable lower limits to the ages for the bulk of the stars in NGC 185, NGC 205, and Fornax (e.g., Hodge 1989; Mould, Kristian, & Da Costa 1984; Eskridge 1987).

4.2. [O/Fe] *and the Formation of Diffuse Ellipticals*

Our estimates of the oxygen abundances in Fornax, NGC 185, and NGC 205 allow us to derive [O/Fe] ratios for the stars in these galaxies. The abundance data are collected in Table 6 along with similar data for stars in the Magellanic Clouds and the Milky Way halo. Unfortunately, the oxygen and iron abundances for Fornax, NGC 185, and NGC 205 in Table 6 do not apply to the same stars. Our oxygen abun-

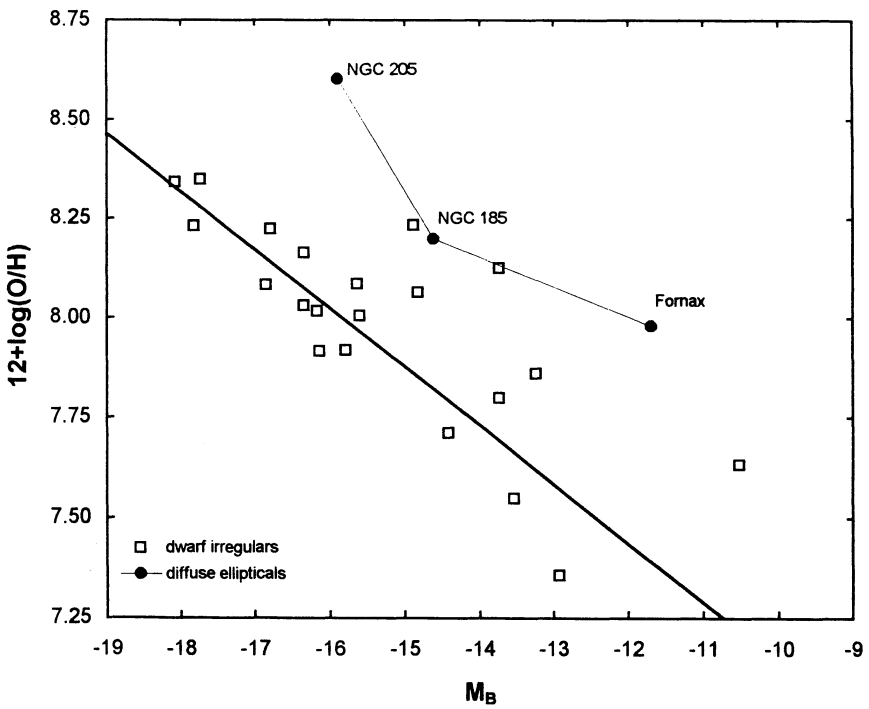

FIG. 4.—Our metallicity-luminosity relation for dwarf irregular galaxies. The open squares represent the dwarf irregulars from Table 5 while the line is a linear least-squares fit to this data for $M_B < -15$. NGC 185, NGC 205, and Fornax are plotted using our preferred abundances (Table 3).

TABLE 6

[O/Fe] IN DIFFUSE ELLIPTICALS

GALAXY	12+log (O/H) (Adopted)	[Fe/H] (dex)[a] Mean	Maximum	Source	μ_1[b]	Z/Z_1[c] (Eq. [4])	[O/H][a]	[O/Fe][a]
Fornax	7.98	−1.40	−0.70	1	...	...	−0.95	−0.25 ± 0.16
NGC 185	8.20	−1.23	−0.90	2	...	...	−0.73	+0.17 ± 0.17
NGC 205	8.60	−0.85	−0.35	3	...	...	−0.33	+0.02 ± 0.21
Fornax	7.98	−1.40	...	1	0.77	0.47	−1.28	+0.12 ± 0.16
NGC 185	8.20	−1.23	...	2	0.56	0.43	−1.10	+0.13 ± 0.19
NGC 205	8.60	−0.85	...	3	0.11	0.27	−0.90	−0.05 ± 0.32
Milky Way halo	8.38	~ −1	...	4	...	...	...	+0.45 ± 0.10
LMC	8.35	−0.30	...	5	...	...	−0.58	−0.28 ± 0.15
SMC	8.03	−0.69	...	5	...	...	−0.90	−0.21 ± 0.16

NOTES.—Abundance sources: (1) Buonanno et al. 1985; (2) Lee, Freedman, & Madore 1993a; (3) Mould, Kristian, & Da Costa 1984; (4) Tomkin et al. 1992; (5) Russell & Dopita 1992.

[a] $[A/B] = \log [n(A)/n(B)] - \log [n(A)/n(B)]_\odot$, $n(X)$ being the number density of element X.

[b] The gas mass fraction when star formation stopped. Calculated using an oxygen yield $y = 0.004$ (see text).

[c] The ratio of the mean stellar oxygen abundance to that when star formation stopped.

dances are those for the most metal-rich stars in these galaxies, but the iron abundances are a mean for all stars. Thus, we must modify one of the abundances to compare them fairly. Since the [O/Fe] ratio contains important information concerning the star formation history, we take two approaches to derive the [O/Fe] ratios.

Our first approach is to modify the iron abundances. When the studies referenced in Table 6 quote a maximum iron abundance, this maximum is given in Table 6. Otherwise, we form a maximum iron abundance by adding the abundance dispersion to the mean abundance. The drawback here is that the reliability of the iron abundance dispersions is unknown. All of these iron abundances are derived from color-magnitude diagrams of stars in these galaxies; thus, although the iron abundances themselves may be reliably determined, observational errors could significantly affect the dispersions. Nonetheless, if we use these maximum iron abundances in the stellar populations for Fornax, NGC 185, and NGC 205, we obtain the first set of [O/Fe] ratios listed in the last column of Table 6. On average, these [O/Fe] ratios are near the solar value. [For comparisons with the Sun, we use the Anders & Grevesse 1989 solar oxygen abundance, 12+log (O/H) = 8.93.]

Our second approach to obtain [O/Fe] ratios is to modify our oxygen abundance estimates. To do this we must rely on chemical evolution models to relate our "last epoch" oxygen abundances to the mean oxygen abundance for all stars. For simplicity, we assume that diffuse ellipticals evolve according to the closed box model until the time when they lose their gas. In this scenario, our oxygen abundances reflect the abundance in the interstellar medium just before the onset of gas loss. In the closed box model, the mass fraction of stars, S, whose abundances by mass, Z, are less than the last-epoch abundances, Z_1, is given by (Audouze & Tinsley 1976, eq. [3])

$$\frac{S}{S_1} = \frac{1 - \mu_1^{Z/Z_1}}{1 - \mu_1}, \tag{5}$$

where S_1 and μ_1 are the last-epoch star and gas mass fractions, respectively. We define the mean stellar oxygen abundance to be the abundance at which the stellar mass fraction is one-half of the total stellar mass fraction, i.e., the abundance for which the right-hand side of equation (5) evaluates to 0.5. To use equation (5), we must estimate the gas mass fraction when the gas was lost. We do this using the relation between the gas mass fraction and the oxygen mass fraction for the closed-box model,

$$Z_1 = y \ln \mu_1^{-1} \tag{6}$$

(Audouze & Tinsley 1976, eq. [1]), where y is the yield of oxygen. Unfortunately, the yield is uncertain, but observations and theoretical studies generally find $0.002 \leq y \leq 0.02$ (e.g., Lequeux et al. 1979; Köppen & Arimoto 1991). Here we use $y = 0.004$, the "observed" value from Lequeux et al. (1979). Fortunately, our choice of yield does not significantly affect the [O/Fe] ratios we derive. Using $y = 0.004$, equation (6) is used to determine the gas mass fraction at which star formation stopped. This gas mass fraction is then used in equation (5) to solve for the mean oxygen abundance for the stars in each galaxy. The resulting values of μ_1, Z/Z_1, and [O/Fe] are listed as the second set of results in Table 6.

The uncertainties assigned to the [O/Fe] ratios in Table 6 are calculated as follows. For oxygen and iron abundances from external sources, the uncertainties quoted in the relevant references were used. For the diffuse ellipticals, the oxygen abundances adopted for the interstellar medium were assigned an uncertainty of 0.06 dex, which is the maximum difference between the actual mean abundance and the lower limits to the mean in the Magellanic Clouds and the Milky Way (Table 3). Finally, the uncertainty assigned to the closed box [O/Fe] ratios allow the yield to vary over the range $0.002 \leq y \leq 0.02$. Only for NGC 205 is the error associated with the yield comparable to those from other sources. Because the oxygen abundance of NGC 205 is high, its final gas mass fraction will be low, so the yield has a larger effect upon the mean oxygen abundance derived from equation (5). The errors associated with the closed box [O/Fe] ratios are slightly asymmetric about the value indicated in Table 6, so only the largest error (negative) is quoted.

Despite the uncertainty in our [O/Fe] ratios for the diffuse ellipticals, it is likely that their true values are distinct from those in the Magellanic Clouds. Figure 5 displays the disparity between the [O/Fe] ratios in the diffuse ellipticals studied here and those in the Magellanic Clouds. Theoretical models of the planetary nebula populations in diffuse ellipticals indicate that the mean oxygen abundance observed in planetary nebulae today underestimates the oxygen abundance that persisted in the interstellar medium when star formation stopped, so the

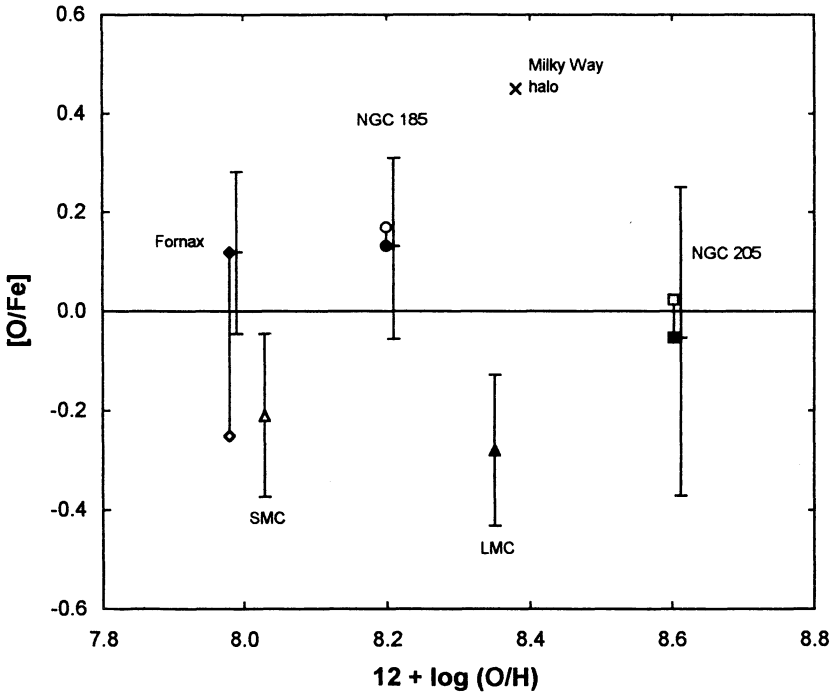

FIG. 5.—Comparison of the [O/Fe] ratios for the diffuse ellipticals studied here and those for the Magellanic Clouds and the Milky Way halo. The filled symbols denote the [O/Fe] ratios for the diffuse ellipticals based upon the closed box model of chemical evolution, while the open symbols denote the [O/Fe] ratios using the maximum [Fe/H]. The plotted error bars include the errors in the oxygen and iron abundances and, for [O/Fe] ratios based upon the closed box model for the diffuse ellipticals, the effect of allowing the yield of oxygen to vary between 0.002 and 0.02. For clarity, the error bars for the diffuse ellipticals are plotted slightly to the right of the closed box [O/Fe] ratios. The horizontal line indicates the solar [O/Fe] ratio.

difference between the [O/Fe] ratios for diffuse ellipticals and dwarf irregulars is actually greater than Figure 5 indicates (Richer, McCall, & Arimoto 1995).

Unfortunately, the Magellanic Clouds are the only dwarf irregulars for which we are aware of [Fe/H] values for the young population, so it is not known whether their [O/Fe] ratios are typical of those in other dwarf irregulars. However, since the time-averaged rate of star formation in dwarf irregulars is low, their [O/Fe] ratios are also expected to be low, though likely with some scatter depending on their exact star formation history (e.g., Gilmore & Wyse 1991). Figure 4 emphasizes that, if dwarf irregulars evolve into diffuse ellipticals, it is dwarf irregulars like the Magellanic Clouds that will evolve into diffuse ellipticals like NGC 185 and NGC 205. Thus, our oxygen abundances argue that diffuse ellipticals have higher [O/Fe] ratios than dwarf irregulars at a given [O/H].

While the oxygen abundance in a galaxy's interstellar medium is a measure of the fraction of that matter that has been turned into stars, the [O/Fe] ratio reflects the rate at which this matter is turned into stars. If the gas is consumed quickly, a high oxygen abundance can build up through the action of Type II supernovae, but the iron abundance can remain low. Consuming the same fraction of gas over a longer timescale produces a lower [O/Fe] ratio since Type I supernovae begin to contribute to the iron production without affecting the oxygen abundance. It would be surprising if the [O/Fe] ratio in diffuse ellipticals were as low as the solar value, since this implies that diffuse ellipticals retained their gas long enough to allow significant iron enrichment from Type I supernovae. However, even if [O/Fe] is as low as the solar value in diffuse ellipticals, this is still sufficiently different from what is observed in the Magellanic Clouds that diffuse ellipticals cannot simply be dwarf irregulars that have lost their gas. Since diffuse ellipticals reach a given oxygen abundance at a higher [O/Fe] than dwarf irregulars, they must have formed stars more rapidly (note that neither galaxy type need consume their gas entirely).

Given their [O/Fe] ratios, it is paradoxical that diffuse ellipticals have no gas (or little gas) whereas dwarf irregulars have significant quantities of gas. At a given oxygen abundance, dwarf irregulars have lower [O/Fe] ratios than diffuse ellipticals, so the total metal content in the interstellar medium is largest for dwarf irrregulars. As a result, the total number of supernovae and the total energy deposited into the interstellar medium by supernovae must be largest for dwarf irregulars. Consequently, the *quantity* of energy deposited cannot be what controls gas loss in diffuse ellipticals. This suggests that the *rate* at which energy is transferred to the interstellar medium may be the important factor regularing gas loss. In addition, decreasing the [O/Fe] ratio at a fixed oxygen abundance increases the total metal content of the gas, enabling it to dissipate the energy input from supernovae more efficiently. Thus, a slow energy transfer rate could enhance the likelihood of retaining gas despite depositing a larger quantity of energy. However, star formation in diffuse ellipticals need not expel the remaining gas. Possibly, the higher energy deposition rates in diffuse ellipticals simply predispose them to other environmental influences that might remove their gas. Conceivably, the difference between a diffuse elliptical and a dwarf irregular lies in the history of star formation. Initially, diffuse ellipticals and dwarf irregulars may be similar, but the star formation process in diffuse ellipticals is sufficiently rapid that they either lose their remaining gas or are predisposed to losing it.

The differences we find between diffuse ellipticals and dwarf irregulars support inferences from photometric studies. From optical photometry, Bothun et al. (1986) found that dwarf irregulars have larger luminosity profile scale lengths and lower surface brightnesses than those of diffuse ellipticals. (The dwarf irregulars in their sample have a larger mean B luminosity than their diffuse ellipticals, so the dwarf irregulars could fade to become diffuse ellipticals.) James (1991) found similar differences between the infrared photometric properties of dwarf irregulars and diffuse ellipticals. Interestingly, Bothun et al. (1986) suggested that blue compact dwarf galaxies have photometric properties that make them suitable precursors to diffuse ellipticals. It is striking that the chief distinguishing characteristic between blue compact dwarfs and dwarf irregulars is that the star formation rates in the former are much higher, exactly in the sense required to make diffuse ellipticals.

5. CONCLUSIONS

We have obtained nebular spectroscopy of planetary nebulae in the dwarf irregular galaxy NGC 6822 and the diffuse ellipticals NGC 185 and NGC 205. For the planetary nebula S33 in NGC 6822, we find an oxygen abundance of $12+\log(\mathrm{O/H}) = 8.10$. We have identified S16 in Killen & Dufour's (1982) catalogue as a new planetary nebula. For this object, we obtain $12+\log(\mathrm{O}^{2+}/\mathrm{H}) = 8.01$ (we observed no lines of O^{+}). In NGC 205, we obtain $12+\log(\mathrm{O}^{2+}/\mathrm{H}) = 8.21$ for PN 2 and $12+\log(\mathrm{O}^{2+}/\mathrm{H}) \geq 8.11$ for PN 5 (again, we observed no lines of O^{+}).

We did not detect the temperature-sensitive [O III] λ4363 line in any other planetary nebulae in NGC 185 or NGC 205, so we developed two empirical techniques to obtain lower limits to their oxygen abundances. These abundance limits are based upon the observations that the maximum attainable [O III] λ5007 luminosities and the [O III] λ5007/Hβ ratios are functions of the oxygen abundance. Tests, using planetary nebulae in the Magellanic Clouds and the Milky Way, show that we obtain the best lower limit to the mean abundance for the whole planetary nebula population if we average the larger of the two lower limits for each individual planetary nebula. However, even this best estimate underestimates the actual mean oxygen abundance in the planetary nebula population by 0.37 dex.

Although these empirical techniques are based upon planetary nebulae in the Magellanic Clouds and the Milky Way, we show that the properties of the planetary nebulae in Fornax, NGC 185, and NGC 205 are not anomalous in any way. Based upon these empirical techniques, our best estimates of the mean oxygen abundances are $12+\log(\mathrm{O/H}) = 8.20$, $12+\log(\mathrm{O/H}) = 8.60$, and $12+\log(\mathrm{O/H}) = 7.98$ for the planetary nebulae in NGC 185, NGC 205, and Fornax, respectively.

We have also introduced a new metallicity-luminosity relation for dwarf irregulars based upon a homogeneous analysis of distance indicators. We find that NGC 185, NGC 205, and Fornax all have oxygen abundances that exceed those of comparably luminous dwarf irregulars by at least 1.5 times the dispersion in the metallicity-luminosity relation. Based upon their distance from the dwarf irregular metallicity-luminosity relation, these galaxies must have faded by 3 to 4 mag if they evolved from dwarf irregulars like those observed today.

When we combine our oxygen abundances with iron abundances in the literature we find that NGC 185, NGC 205, and Fornax have [O/Fe] ratios that, on average, are near or somewhat larger than the solar value. Such [O/Fe] ratios are significantly larger than those of dwarf irregulars. The simplest explanation is that diffuse ellipticals consume their gas more rapidly than dwarf irregulars before expelling or losing what remains of it. We suggest that the rapidity with which diffuse ellipticals consume their gas may be the key difference between them and dwarf irregulars. Consequently, diffuse ellipticals cannot be the faded remnants of dwarf irregulars since their star formation histories are fundamentally different.

The authors would like to thank the staffs at the Multiple Mirror Telescope and the Canada-France-Hawaii Telescope, particularly Olivier LeFévre, for their able assistance with the observations. M. G. R. would like to thank the Ontario Ministry of Colleges and Universities and Marshall McCall for financial support. M. L. M. would like to thank the Natural Sciences and Engineering Research Council of Canada for its continuing support.

APPENDIX

DISTANCES TO LOCAL DWARF GALAXIES

A1. INTRODUCTION

Research into local dwarfs hinges upon reliable distances because peculiar motions are large enough that relative distances cannot be judged from radial motions. Unfortunately, such distances are hard to come by. When distances are available, users tend to adopt published values without regard to their background. If more than one estimate is available for a given galaxy, these estimates are often averaged without regard to whether they are self-consistent. Inconsistencies may result, for example, from different choices for the galactic extinction, reddening law, or zero point (such as the distance to the LMC). Some measurements in Kron-Cousins R or I are even corrected for extinction using coefficients for Johnson R and I. Consequently, studies of local dwarf galaxies are often plagued, and, in the worst cases, biased, by scatter contributed by inhomogeneous distances.

As part of a long-term study of the Galactic neighborhood, an effort has been made to homogenize and refine the distances to local dwarfs. Given the breakdown of the Tully-Fisher relation at low luminosities, distances have been based only upon indicators tied to stellar constitutents, or the distance to an associated group in which there is a galaxy for which a distance is tied directly to stellar constitutents. In fact, in this paper, galaxies lacking such a distance were rejected from the sample.

All distance indicators have been tied to common origins. The latest available data have been employed in deriving distance moduli. Where available, direct measures of extinction have been adopted. Rigorous account has been taken of the color dependencies of $E(B-V)$ and the ratio of total-to-selective extinction in broadband filters following the foundations laid by Laney &

Stobie (1993). The entire distance system is managed within a spreadsheet, wherein an update to any pillar is automatically propagated to all galaxies.

What follows is a brief description of the foundations of the techniques employed to determine the distances used in this paper. A more detailed account of distance determinations for individual galaxies will be published in a future paper. For uncertainties in the methods, the reader should refer to the developmental papers.

A2. THE LMC

Distances to many local galaxies are measured with respect to the LMC. Thus, a reliable distance is essential. The best distance to the LMC is that derived from the ring around SN 1987A (see Panagia et al. 1991). The best estimates for the angular size of the ring (Plait et al. 1994) and the time of the second caustic (Gould 1994) place the supernova at a distance modulus of 18.346 ± 0.040. The supernova is 0.026 ± 0.035 mag closer to the Milky Way than the center of mass of the LMC (McCall 1993, but with the error in the sign of the tilt of the LMC corrected). The uncertainty covers the effect of allowing the supernova to lie at any depth within the layer confining 99% of the light of the young disk. Thus, the adopted distance modulus for the LMC is

$$\mu_{\rm LMC} = 18.372 \pm 0.053 \, . \tag{7}$$

A3. M31

Some dwarf distances are tied to the distance of M31. The best distance to M31 is provided by multicolor photometry of Cepheids (Freedman & Madore 1990), which yields the position relative to the LMC. This technique permits a solution for the distance modulus which is free of the extinction of the very Cepheids under study. Based upon the data of Freedman & Madore (1990), the adopted LMC distance leads to a distance modulus for M31 given by

$$\mu_{\rm M31} = (24.286 \pm 0.082) + (\mu_{\rm LMC} - 18.372) \, . \tag{8}$$

A4. M81

In this work, distances based upon the brightest blue and red stars are founded upon the distance to the M81 group. As for M31, the adopted value comes from multicolor observations of Cepheids in M81 (Madore, Freedman, & Lee 1993) with respect to the LMC:

$$\mu_{\rm M81} = (27.65 \pm 0.21) + (\mu_{\rm LMC} - 18.372) \, . \tag{9}$$

A5. CEPHEID VARIABLES

The zero points of Cepheid period-luminosity relations are not well known, so distances from Cepheids are usually measured with respect to the LMC. When available, distances derived from multicolor observations of Cepheids are preferred, owing to the simultaneous accounting for extinction. When data are available in only one passband, the merit of the indicator is weighed with respect to other methods. In all cases, distances are set using the adopted distance to the LMC.

A6. RR LYRAE STARS AND THE HORIZONTAL BRANCH

Observations of RR Lyrae stars and the horizontal branch are helpful in determining the distance to dwarfs which have not formed stars recently. Care must be taken to account for the sensitivity of the absolute magnitude to metallicity. Walker (1992) has summarized data for cluster RR Lyrae stars in the LMC, from which a zero point for absolute magnitudes can be derived. Assuming that absolute magnitudes depend upon metallicity in the manner advocated by Carney, Storm, & Jones (1992), the intensity mean absolute magnitude of RR Lyrae stars in V is given by

$$\langle M_V \rangle = 0.15[{\rm Fe/H}] + 0.880 - (\mu_{\rm LMC} - 18.372) \, . \tag{10}$$

In this work, the absolute magnitude of the horizontal branch is equated with the mean absolute magnitude of RR Lyrae stars.

A7. TIP OF THE RED GIANT BRANCH

Recently, it has been demonstrated that the absolute I magnitude of the tip of the red giant branch is a good distance indicator (Lee, Freedman, & Madore 1993a). In the past, the calibration has been tied to RR Lyrae absolute magnitudes and theoretical estimates of bolometric corrections. It is preferable to force the distance of M31 to agree with the value adopted above. With the metallicity sensitivity of RR Lyrae absolute magnitudes as above, the absolute magnitude of the tip of the red giant branch in Kron-Cousins I is given by

$$M_I = M_{I,{\rm M31}} + 0.243[(V-I)^0 - (V-I)^0_{\rm M31}] - 0.21([{\rm Fe/H}] - [{\rm Fe/H}]_{\rm M31}) \, , \tag{11}$$

where $(V-I)^0$ is the reddening-free $(V-I)$ color and [Fe/H] is the iron abundance relative to the Sun for the stars at the tip. The relation is calibrated using the following parameters for the tip of the red giant branch in M31 (Lee, Freedman, & Madore 1993a;

Mould & Kristian 1986), which are linked to the adopted distance:

$$M_{I,\mathrm{M31}} = -3.881 - (\mu_{\mathrm{M31}} - 24.286)\,, \qquad (V-I)^0_{\mathrm{M31}} = 1.843\,, \qquad [\mathrm{Fe/H}]_{\mathrm{M31}} = -0.8\,. \tag{12}$$

A8. SURFACE BRIGHTNESS FLUCTUATIONS

Distances based upon surface brightness fluctuations (Tonry 1991; Tonry & Schechter 1990) are available for the bulges of nearby spirals with which dwarfs are associated, as well as for a few diffuse and dwarf ellipticals. They are anchored to the distance of M31. The mean absolute magnitude of fluctuations in Kron-Cousins I is given by

$$\langle M_I \rangle = \langle M_{I,\mathrm{M31}} \rangle + 3.0[(V-I)^0 - (V-I)^0_{\mathrm{M31}}]\,, \tag{13}$$

where $(V-I)^0$ is the reddening-free $(V-I)$ color of the *galaxy* where the fluctuations are measured (not the color of the fluctuations). The relation is calibrated using the following parameters for surface brightness fluctuations in M31, which are linked to the adopted distance:

$$\langle M_{I,\mathrm{M31}} \rangle = -1.150 - (\mu_{\mathrm{M31}} - 24.286)\,, \qquad (V-I)^0_{\mathrm{M31}} = 1.170\,. \tag{14}$$

A9. PLANETARY NEBULAE

The luminosity function of planetary nebulae in the light of [O III] λ5007 is universal enough that the brightest planetary nebulae in galaxies can be used as a distance indicator (Jacoby 1989; Ciardullo et al. 1989). Planetary nebulae in the bulge of M31 and in the LMC are among the best studied. Here, distances are anchored to M31 (Ciardullo et al. 1989), and the metallicity sensitivity is derived using the planetary nebulae in the LMC (Richer 1993, eq. [1]). The absolute magnitude of the brightness limit of the luminosity function is given by

$$M^*_{5007} = M^*_{5007,\mathrm{M31}} + 0.750x^2 - 13.675x + k\,, \tag{15}$$

where $x = 12 + \log n(\mathrm{O})/n(\mathrm{H})$ is the actual oxygen abundance by number, and k is a constant derived from the properties of the planetary nebulae in the LMC. From Ciardullo et al. (1989),

$$M^*_{5007,\mathrm{M31}} = -4.444 - (\mu_{\mathrm{M31}} - 24.286)\,. \tag{16}$$

The zero point in equation (15) can be set by computing the value of M^*_{5007} corresponding to any particular oxygen abundance. Thus, given the adopted distance to the LMC and its foreground reddening of 0.035 mag (McNamara & Feltz 1980) and using the Schild (1977) reddening law adjusted to a ratio of total-to-selective extinction $R = 3.07$, for $x_{\mathrm{LMC}} = 8.33$,

$$M^*_{5007} = -4.055 - (\mu_{\mathrm{LMC}} - 18.372)\,, \tag{17}$$

so

$$k = 62.260 \text{ mag}\,. \tag{18}$$

A10. BRIGHTEST BLUE STARS

Sandage & Tammann (1974) pioneered the use of the brightest three blue stars in a galaxy to estimate distances. This method is inferior to the previous methods described and fails in galaxies lacking active star formation, but often it is the only way that the distance to a dwarf can be determined. The main problem with its application is that the absolute magnitude of the brightest blue stars is tied to the luminosity of the host, primarily for statistical reasons. To calibrate this indicator, galaxies in the M81/NGC 2403 group have been examined. By restricting the analysis to galaxies in a group, scatter due to distance errors is reduced. Also, because it is possible to adopt a common distance for all galaxies, the calibration can be directly linked to the distance of a single galaxy (the one with the best determined distance, i.e., M81).

Measurements of bright stars in the M81/NGC 2403 group summarized by Karachentsev & Tikhonov (1994) (corrected for galactic extinction, and, in the case of stars in galaxies with a stage earlier than $T = 10$, for extragalactic extinction via a cosecant law) have been used with apparent total magnitudes from de Vaucouleurs et al. (1991) and Pierce & Tully (1992) (all galaxies corrected for galactic extinction and galaxies with stages earlier than 10 corrected for extragalactic extinction using the algorithm of Tully & Fouqué 1985 as applied by McCall 1995) to derive a relationship between the absolute magnitude of a galaxy, M_B, and the corrected mean apparent magnitude of the brightest three blue stars in B, $\langle B(3) \rangle^0$, relative to the corrected total magnitude of the galaxy in B, B^0_T. With the zero point set by the adopted distance to M81, the result is

$$\langle B(3) \rangle^0 - B^0_T = -0.6531 M_B - 2.618 - 0.6531(\mu_{\mathrm{M81}} - 27.65)\,. \tag{19}$$

Thus, one can use the apparent magnitude of the brightest blue stars to solve for the absolute magnitude of a galaxy and thereby determine the distance. The absolute magnitude of the brightest three blue stars is given by

$$\langle M_B(3) \rangle = 0.3469 M_B - 2.618 + 0.3469(\mu_{\mathrm{M81}} - 27.65)\,. \tag{20}$$

A11. BRIGHTEST RED STARS

Sandage & Tammann (1974) also pioneered the use of the three brightest red stars as a distance indicator, the mean absolute magnitude of which appears to be relatively constant. However, the method fails in systems lacking recent star formation, at which point giants can be mistaken for supergiants. Again the M81/NGC 2403 group has been used to calibrate this indicator. After correcting for extinction in the manner described for the brightest blue stars, the mean absolute magnitude of the brightest three red stars in dwarfs fainter than the SMC is given by

$$\langle M_V(3)\rangle = -7.65 - (\mu_{\rm M81} - 27.65) \qquad (M_B > -17)\,. \tag{21}$$

A12. CARBON STARS

Carbon stars have been suggested on empirical grounds to be a standard candle (Richer 1981; Pritchet et al. 1987). Although carbon stars have not been widely applied to determine distances, there are a few observations of particular value to the determination of distances to local dwarfs. Distances are linked to the LMC. Using the adopted distance to the LMC, the mean absolute magnitude of carbon stars in Kron-Cousins I is

$$\langle M_I\rangle = -4.72 - (\mu_{\rm LMC} - 18.372)\,. \tag{22}$$

REFERENCES

Aller, L. H., & Keyes, C. D. 1987, ApJS, 65, 405
Anders, E., & Grevesse, N. 1989, Geochim. Cosmichim. Acta, 53, 197
Anderson, E. 1987, Reduction of Long-Slit Spectroscopic Data Using IRAF, IRAF User Handbook, Vol. 2B (Tucson: National Optical Astronomy Obs.)
Aparicio, A., Garcia-Pelaya, J. J., & Moles, M. 1988, A&AS, 74, 375
Audouze, J., & Tinsley, B. M. 1976, ARA&A, 14, 43
Binggeli, B., & Cameron, L. M. 1992, A&A, 252, 27
Binggeli, B., Tammann, G. A., & Sandage, A. 1987, AJ, 94, 251
Blades, J. C., et al. 1992, ApJ, 398, L41
Bothun, G. D., Mould, J. R., Caldwell, N., & MacGillivray, H. T. 1986, AJ, 92, 1007
Bruzual, G. A., & Charlot, S. 1993, ApJ, 405, 538
Buonanno, R., Corsi, C. E., Fusi Pecci, F., Hardy, E., & Zinn, R. 1985, A&A, 152, 65
Burstein, D., & Heiles, C. 1984, ApJS, 54, 33
Carney, B. W., Storm, J., & Jones, R. V. 1992, ApJ, 386, 663
Ciardullo, R. C., Jacoby, G. H., Ford, H. C., & Neill, J. D. 1989, ApJ, 339, 53
Davidge, T. J. 1992, ApJ, 397, 457
Dekel, A., & Silk, J. 1986, ApJ, 303, 39
De Robertis, M. M., Dufour, R. J., & Hunt, R. W. 1987, JRASC, 81, 195
de Vaucouleurs, G., de Vaucouleurs, A., Corwin, H. G., Jr., Buta, R. J., Paturel, G., & Fouqué, P. 1991, Third Reference Catalogue of Bright Galaxies (New York: Springer)
Dopita, M. A., Jacoby, G. H., & Vassiliadis, E. 1992, ApJ, 389, 27
Dufour, R. J., & Talent, D. L. 1980, ApJ, 235, 22
Eskridge, P. B. 1987, AJ, 94, 1564
Ferland, G. J. 1991, Hazy: A Brief Introduction to CLOUDY 80.05 (OSU Astronomy Dept. Internal Rept. 91-01)
Ford, H. C., & Jacoby, G. H. 1978, ApJ, 219, 413
Ford, H. C., Jenner, D. C., & Epps, H. W. 1973, ApJ, 183, L73
Freedman, W. L. 1988, ApJ, 326, 691
Freedman, W. L., & Madore, B. F. 1990, ApJ, 365, 186
French, H. B. 1980, ApJ, 240, 41
Gilmore, G., & Wyse, R. F. G. 1991, ApJ, 367, L55
Gonzalez-Riestra, R., Rego, M., & Zamorano, J. 1988, A&A, 202, 27
Gould, A. 1994, private communication
Henry, R. B. C. 1989, MNRAS, 241, 453
Heydari-Meyalari, M., Melnick, J., & Martin, J.-M. 1990, A&A, 234, 99
Hodge, P. W. 1989, ARA&A, 27, 139
Hui, X., Ford, H. C., Ciardullo, R., & Jacoby, G. H. 1993, ApJ, 444, 463
Iben, I., Jr., & Renzini, A. 1983, ARA&A, 21, 271
Jacoby, G. H. 1989, ApJ, 339, 39
Jacoby, G. H., & Ford, H. C. 1986, ApJ, 304, 490
Jacoby, G. H., & Kaler, J. B. 1993, ApJ, 417, 209
Jacoby, G. H., Walker, A. R., & Ciardullo, R. 1990, ApJ, 365, 471
James, P. 1991, MNRAS, 250, 544
Kaler, J. B. 1994, 22d General Assembly of the International Astronomical Union, 1994 August 15–27 (Den Haag, The Netherlands)
Karachentsev, I. D., & Tikhonov, N. A. 1994, A&A, in press
Kennicutt, R., Balick, B., & Heckman, T. 1980, PASP, 92, 134
Killen, R. M., & Dufour R. J. 1982, PASP, 94, 444
Kingsburgh, R. L. 1992, Ph.D. thesis, Univ. College London
Kinman, T. D., & Davidson, K. 1981, ApJ, 243, 127
Kohoutek, L., & Martin, W. 1981, A&AS, 44, 325
Köppen, J., & Arimoto, N. 1991, A&AS, 87, 109
Kormendy, J. 1985, ApJ, 295, 73
Kormendy, J., & Djorgovski, S. 1989, ARA&A, 27, 235
Laney, C. D., & Stobie, R. S. 1993, MNRAS, 263, 921
Le Fèvre, O., Crampton, D., Felenbock, P., & Monnet, G. 1994, A&A, 282, 325
Lee, M. G. 1993, ApJ, 408, 409
Lee, M. G., & Madore, B. F. 1993, AJ, 106, 66
Lee, M. G., Freedman, W. L., & Madore, B. F. 1993a, ApJ, 417, 553
———. 1993b, in IAU Colloq. 139, New Perspectives on Stellar Pulsation and Pulsating Variable Stars, ed. J. Nemec (Cambridge: Cambridge Univ. Press), in press
Lequeux, J., Peimbert, M., Rayo, J. F., Serrano, A., & Torres-Peimbert, S. 1979, A&A, 80, 155
Madore, B. F., & Freedman, W. L. 1991, PASP, 103, 933
Madore, B. F., Freedman, W. L., & Lee, M. G. 1993, AJ, 106, 2243
Maran, S. P., Gull, T. R., Stecher, T. P., Aller, L. H., & Keyes, C. D. 1984, ApJ, 280, 615
Masegosa, J., Moles, M., & del Olmo, A. 1991, A&A, 249, 505
Massey, P., Valdes, F., & Barnes, J. 1992, A User's Guide to Reducing Slit Spectra with IRAF, IRAF User Guide, Vol. 2B (Tucson: National Optical Astronomy Obs.)
Masson, C. R. 1989, ApJ, 336, 294
McAlary, C. W., & Welch, D. L. 1985, in IAU Colloq. 82, Cepheids: Theory and Observations, ed. B. F. Madore (Cambridge: Cambridge Univ. Press), 228
McCall, M. L. 1982, Ph.D. thesis, Univ. of Texas; also Univ. of Texas Publ. 20
———. 1993, ApJ, 417, L75
———. 1995, MNRAS, submitted
McClure, R. D., & Racine, R. 1969, AJ, 74, 1000
McNamara, D. H., & Feltz, K. A., Jr. 1980, PASP, 92, 587
Meatheringham, S. J., & Dopita, M. A. 1991a, ApJS, 75, 407
———. 1991b, ApJS, 76, 1085
Méndez, R. H., Kudritzki, R. P., Ciardullo, R., & Jacoby, G. H. 1993, A&A, 275, 534
Méndez, R. H., Kudritzki, R. P., & Herrero, A. 1992, A&A, 260, 329
Moles, M., Aparicio, A., & Masegosa, J. 1990, A&A, 228, 310
Mould, J., & Kristian, J. 1986, ApJ, 305, 591
Mould, J., Kristian, J., & Da Costa, G. S. 1984, ApJ, 278, 575
Osterbrock, D. E. 1989, Astrophysics of Gaseous Nebulae and Active Galactic Nuclei (Mill Valley: University Science)
Pagel, B. E. J., Edmonds, M. G., & Smith, G. 1980, MNRAS, 193, 219
Panagia, N., Gilmozzi, R., Macchetto, F., Adorf, H.-M., & Kirshner, R. P. 1991, ApJ, 380, L23
Peimbert, M., Pena, M., & Torres-Peimbert, S. 1986, A&A, 158, 266
Peimbert, M., & Spinrad, H. 1970, A&A, 7, 311
Peimbert, M., & Torres-Peimbert, S. 1983, in IAU Symp. 103, Planetary Nebulae, ed. D. R. Flower (Dordrecht: Reidel), 233
Pierce, M. J., & Tully, R. B. 1992, ApJ, 387, 47
Plait, P., Lundqvist, P., Chevalier, R., & Kirshner, R. P. 1994, preprint
Pritchet, C. J., Richer, H. B., Schade, D., Crabtree, D., & Yee, H. K. C. 1987, ApJ, 323, 79
Renzini, A., & Buzzoni, A. 1986, in Spectral Evolution of Galaxies, ed. C. Chiosi, & A. Renzini (Dordrecht: Reidel), 195
Richer, H. B. 1981, ApJ, 243, 744
Richer, M. G. 1993, ApJ, 415, 240
Richer, M. G., McCall, M. L., & Arimoto, N. 1995, in preparation
Russell, S. C., & Dopita, M. A. 1992, ApJ, 384, 508
Saha, A., & Hoessel, J. G. 1990, AJ, 99, 97
Saha, A., Hoessel, J. G., & Krist, J. 1992, AJ, 103, 84
Sandage, A. 1986, AJ, 91, 496
Sandage, A., & Tammann, G. A. 1974, ApJ, 190, 525
———. 1982, ApJ, 256, 339

Schild, R. E. 1977, AJ, 82, 337
Skillman, E. D., Kennicutt, R. C., &Hodge, P. W. 1989a, ApJ, 347, 875
Skillman, E. D., Melnick, J., Terlevich, R., & Moles, M. 1988, A&A, 196, 31
Skillman, E. D., Terlevich, R., & Melnick, J. 1989b, MNRAS, 240, 563
Stasinska, G., Comte, G., & Vigroux, L. 1986, A&A, 154, 352
Talent, D. L. 1980, Ph.D. thesis, Rice Univ.
Terlevich, R., Melnick, J., Masegosa, J., Moles, M., & Copetti, M. V. F. 1991, A&AS, 91, 285
Tomkin, J., Lemke, M., Lambert, D. L., & Sneden, C. 1992, AJ, 104, 1568
Tonry, J. L. 1991, ApJ, 373, L1
Tonry, J. L., & Schechter, P. 1990, AJ, 100, 1794
Torres-Peimbert, S., & Peimbert, M. 1977, Rev. Mexicana Astron. Af., 2, 181
Tully, R. B., Boesgaard, A. M., Dyck, H. M., & Schempp, W. V. 1981, ApJ, 246, 38
Tully, R. B., & Fouqué, P. 1985, ApJS, 58, 67
van den Bergh, S. 1969, ApJS, 19, 145
van den Bergh, S., & Humphreys, R. M. 1979, AJ, 84, 604
Vassiliadis, E., Dopita, M. A., Morgan, D. H., & Bell, J. F. 1992, ApJS, 83, 87
Vigroux, L., Stasinska, G., & Comte, G. 1987, A&A, 172, 15
Walker, A. R. 1992, ApJ, 390, L81
Webster, B. L. 1988, MNRAS, 230, 377
Webster, B. L., & Smith, M. G. 1983, MNRAS, 204, 743
Wheeler, J. C., Sneden, C., & Truran, J. W., Jr. 1989, ARA&A, 27, 279
Wirth, A., & Gallagher, J. S., III, 1984, ApJ, 282, 85